DMTO – a method for Discrete Material and Thickness Optimization of laminated composite structures

Sørensen, Søren Nørgaard; Sørensen, Rene; Lund, Erik

Published in:
Structural and Multidisciplinary Optimization

DOI (link to publication from Publisher):
10.1007/s00158-014-1047-5

Publication date:
2014

Document Version
Early version, also known as pre-print

DMTO – a method for Discrete Material and Thickness Optimization of laminated composite structures

Søren N. Sørensen[1], René Sørensen[2], and Erik Lund[3]

[1,2,3]Department of Mechanical and Manufacturing Engineering, Aalborg University, Fibigerstraede 16, DK-9220 Aalborg East, Denmark, [1]sns@-tech.aau.dk, [2]rso@-tech.aau.dk

May 2014

Abstract

This paper presents a gradient based topology optimization method for Discrete Material and Thickness Optimization of laminated composite structures, labelled the DMTO method. The capabilities of the proposed method are demonstrated on mass minimization, subject to constraints on the structural criteria; buckling load factors, eigenfrequencies, and limited displacements. Furthermore, common design guidelines or rules, referred to as manufacturing constraints, are included explicitly in the optimization problem as series of linear inequalities. The material selection and thickness variation are optimized simultaneously through interpolation functions with penalization. Numerical results for several parameterizations of a finite element model of a generic main spar from a wind turbine blade are presented. The different parameterizations represent different levels of complexity with respect to manufacturability. The results will thus give insight into the relation between potential weight saving and design complexity. The results show that the DMTO method is capable of solving the problems robustly with only few intermediate valued design variables.

1 Introduction

Today, laminated composites are used in a wide variety of weight critical products, ranging from recreational items like badminton rackets and mountain bikes, to large industrial structures such as airplanes and wind turbines. Designing such structures is not a straightforward task as it requires considerations regarding e.g., available materials, demands for performance, manufacturing methods, and common design guidelines or rules, referred to as manufacturing constraints. As a consequence of these criteria, the design process is typically iterative and time consuming. From an engineering perspective, one way of systematically addressing such a design process is to use a suitable optimization method. In this paper, we present a gradient based topology optimization method for mass minimization of laminated composite structures by the simultaneous determination of material distribution and thickness variation. The method is labelled Discrete Material and Thickness Optimization (DMTO), being an immediate extension of the original DMO method by Stegmann and Lund (2005). Mass minimization reduces material expenses and issues related to the net weight of the structure. Mass is minimized subject to constraints on the following structural criteria; buckling load factors, eigenfrequencies, and limited displacements. Furthermore, series of so-called manufacturing constraints (MC's) are considered as a means to fulfill experience based design guidelines or rules for laminated composite structures.

As the DMTO name suggests, the laminate thickness should preferably add up to a discrete number of plies with predefined thicknesses. The number of plies must naturally be able to vary throughout the structure to facilitate mass reduction. The material selection is conducted among a discrete set of material candidates, and should preferably result in a distinct choice rather than a mixture between two or more candidates. Intermediate valued, continuous variables, are penalized as the means to obtain the preferred discreteness. This classical density approach is elaborated in the following section. The candidates may consist of any material, as it is merely required to input the effective constitutive properties and density. It is thus possible to choose among the same orthotropic material with different fiber orientations, biax-angle fiber materials, foam and wood materials, or even customized Non Crimp Fabrics (NCF's) and prepregs. This selection among a discrete set of candidates resembles the current production technology of several laminated composite structures. In the wind turbine industry, the material candidates are typically placed, rolled out, or stacked in a mold where they are processed using vacuum infusing techniques.

Material optimization on basis of a discrete set of candidates for structures with constant laminate thickness has attracted much attention in the last decades. Most contributions on this topic have been summarized in Ghiasi et al. (2009). In the original DMO method, the

selection of a distinct material candidate was achieved by balancing the different design variables such that an increase in one would automatically decrease remaining ones, see Lund and Stegmann (2005). More recently, Hvejsel et al. (2011) considered alternative strategies for discrete multi-material stiffness optimization and proposed series of linear equality constraints to prevent the total sum of the candidate design variables from exceeding unity within each design domain. In order to obtain discrete designs, i.e., the distinct selection of exactly one of the candidates, the authors furthermore proposed a quadratic penalty constraint to gradually force the design variables to their discrete bounds. As an alternative to this non-linear penalty constraint, Hvejsel and Lund (2011) formulated multi-material variations of the SIMP and RAMP interpolation schemes, see Bendsøe (1989) and Stolpe and Svanberg (2001), respectively. As an alternative to the DMO schemes, Bruyneel (2011) introduced the Shape Functions with Penalization (SFP) scheme. The SFP scheme is based on the shape functions of a quadrangular first order finite element, using only two natural coordinates to interpolate between four material candidates. The method was later extended to also include three and eight node elements, see Bruyneel et al. (2011). Gao et al. (2012) proposed a Bi-valued Coding Parameterization (BCP) scheme which distinguishes itself from SFP schemes in that it does not have a limit on the number of applied material candidates. SFP and BCP schemes reduce the number of required design variables compared to DMO schemes. We finally mention Kennedy and Martins (2013) that proposed a series of non-linear equality constraints, which were added as a penalty term to the objective function, thereby penalizing intermediate valued design variables. The above mentioned methods are capable of optimizing the material distribution throughout a laminated composite with constant total thickness. Thus, allowing for determining either an optimum stacking sequence or a sandwich design throughout the predefined and fixed number of layers. Most methods have traditionally been demonstrated on mass constrained minimization of compliance. However, recent advances within the field have likewise been demonstrated on eigenfrequency problems, see e.g., Lund and Stegmann (2005) and Niu et al. (2010), and also problems considering buckling load factors have been attracting more attention, see e.g., Lund (2009) and Kennedy and Martins (2013).

Literature concerning optimization of multilayered laminated composite structures with variable total thickness is more limited. Ghiasi et al. (2010) reviews work on variable stiffness designs, with only few references concerning variable thickness. Manne and Tsai (1998) utilized plydrop tapering for thickness optimization of symmetric layups to avoid warping. Toropov et al. (2005) applied a Genetic Algorithm (GA) to minimize the mass of a monolithic composite wing rib model using discrete fiber orientations and the number of plies as design variables. Most approaches on variable laminate thickness optimization divide the optimization process into multiple phases where thickness and material determination are handled separately. Liu et al. (2011) presented a two phase or bi-level method for minimizing the mass of composite wing panels subject to strain constraints. In the first phase, the number of $\{-45°, 0°, 45°, 90°\}$ plies was determined, and in the second phase a GA was utilized to shuffle the placement of plies in order to accommodate common design rules used in the aerospace industry. The approach applied by Altair Engineering in the commercial software OptiStruct relies on three distinct phases, see Zhou et al. (2011) and Zhou and Fleury (2012). Phase I concerns the conceptual ply layout; Phase II determines the specific number of plies; Phase III determines the final stacking sequence of the laminate, taking into account performance demands and the previously mentioned manufacturing constraints. The method proposed in this paper considers thickness and material determination simultaneously, explicitly taking into account performance demands and manufacturing constraints throughout the process.

The addition of manufacturing constraints in laminate design optimization has attracted more attention as the optimization methods have evolved. Manufacturing constraints represent common design guidelines or rules formulated to e.g., reduce the risk of local failure in the structure. These failure modes are typically associated with out-of-plane stresses that are not captured with a sufficient level of detail when using standard shell elements in a finite element context. In order to capture these effects, a 3D-solid finite element model could be applied. Such detailed modeling is, however, seldom applied in optimization frameworks, given a substantial computational time. Hence, manufacturing constraints serve as an effective way of implicitly considering these effects, and thus obtain designs that require less time for manual post-processing. Generally, the constraints typically found in the literature have their origins in the aerospace industry, see Kassapoglou (2010). Manufacturing constraints can furthermore be used to limit the complexity of the optimized design, thus making it possible to achieve a higher degree of manufacturability. In this work, four common manufacturing constraints, denoted MC1-MC4, introduced in the previous work by Sørensen and Lund (2013), are considered. MC1 is not an explicit constraint as it is related to the design parameterization. In short, MC1 concerns the possible arrangement or grouping of small finite element domains into larger domains, adequate for the allowable variation in both candidate selection and thickness. MC2 explicitly limits the thickness variation rate between adjacent design regions to reduce the risk of delamination. Costin and Wang (1993) formulated a similar constraint in the case where the individual laminae thicknesses are applied as continuous design variables. MC3 limits the number of identical contiguous

layers through the thickness to reduce the risk of matrix cracking. This type of constraint has been investigated by e.g., Le Riche and Haftka (1993), Liu et al. (1999), Toropov et al. (2005), and Liu et al. (2011) in the context of stacking sequence optimization with GA's. Also, Bruyneel et al. (2012) included this constraint for discrete material optimization with constant thickness. MC4 prevents intermediate void from appearing through the thickness of the laminate. MC1-MC4 are all formulated as linear constraints, which makes them efficient to fulfill for the optimizer. The constraints are elaborated in Section 2.3.

Several other manufacturing constraints occur in the literature such as requirements for e.g., symmetric and balanced laminates, minimum proportion or presence of candidates, and so-called adjacency constraints or blending rules to limit the in-plane change in fiber orientation, see e.g., Seresta et al. (2007), Kassapoglou (2010), Zein et al. (2012), Bruyneel et al. (2012), and Kennedy and Martins (2013). In spite of the clear relevance of the above mentioned manufacturing constraints, these particular constraints are not explicitly considered in the DMTO method to be presented here. The formulation and inclusion of such constraints are hence left for future work on the DMTO method. Other potential manufacturing constraints which would be of interest would be a type of sandwich constraint, ensuring that core material is always enclosed by layers of fiber material. The necessity of one such sandwich constraint is discussed in Section 5. As mentioned, manufacturing constraints are mainly included to reduce the risk of out-of-plane failure modes. In-plane failure modes could potentially be monitored by including local strength criteria such as e.g., max stress and max strain constraints or other criteria such as the Tsai-Wu failure criterion, see Tsai and Wu (1971), Kim et al. (1994), and Groenwold and Haftka (2006). In the context of topology optimization with isotropic materials, stress constraints have been investigated by Duysinx and Sigmund (1998) and more recently by Le et al. (2010), París et al. (2010), and Bruggi and Duysinx (2012). The formulation and inclusion of local constraints within gradient based, multi-material topology optimization is currently being investigated by e.g., Lund et al. (2013), but is not yet a mature technology. Despite of the obvious relevance, local criteria are not considered here but left for future work.

The method proposed in this work is a continuation of the work by Sørensen and Lund (2013) who presented a novel method for simultaneous determination of material distribution and thickness variation of multilayered laminated composite structures. The preceding method was demonstrated on simply parameterized monolithic laminated plates with various boundary conditions, where the objective was to minimize compliance subject to a mass/volume constraint and manufacturing constraints MC1-MC4. Compared to the preceding work, we are now considering multi-material topology optimization. Likewise, we change focus from minimum compliance optimization to minimizing mass subject to the following structural performance constraints; buckling load factors, eigenfrequencies, and limited displacements. Mass minimization is viewed as an industrially more relevant problem, as the mass can be directly related to the cost of the final product. Together with the manufacturing constraints MC1-MC4, this is altogether constituting a far more difficult problem. The additional difficulties arise from the presence of the non-linear and non-convex structural constraint functions. In order to manage these difficulties, we present a new procedure for obtaining near discrete design. The capabilities of the DMTO approach are demonstrated on several parameterizations of a finite element model of a generic main spar from a wind turbine blade. The different parameterizations show the flexibility of the proposed method, but also represent different levels of complexity with respect to manufacturability. The results will thus give insight into the relation between potential weight saving and design complexity.

It is noticed that DMTO results should not be viewed as final designs, ready to manufacture, as the final design may still need some amount of manual post-processing despite the inclusion of certain manufacturing constraints. There are several reasons for this, of which one is related to the assumption that adjacent layers with different fiber orientations are perfectly bonded. These regions are typically manufactured by introducing a certain amount of in-plane overlap between the two fiber materials and require detailed analysis. Likewise, the optimized structure may be part of a larger assembly of other sub-structures. Hence, jointing and other detailed considerations with regards to assembly have to be done post to the optimization procedure. Thus, the optimized results should rather serve as a vital source of inspiration for thickness variation and stacking sequences throughout the entire structure, taking into account the complexity of elastic couplings and demands on structural performance as well as manufacturing constraints.

The paper is organized as follows. Section 2 explains the DMTO method in detail, covering areas regarding the design parameterization, the applied density approach, the considered manufacturing constraints MC1-MC4, the mathematical formulation including sensitivity analysis, the Sequential Linear Programming (SLP) approach, and a simple rounding technique to finalize the optimized results. Section 3 introduces several numerical examples concerning a finite element model of a generic main spar from a wind turbine blade. Numerical results are presented in Section 4 and discussed in Section 5. The paper is finalized with conclusions in Section 6.

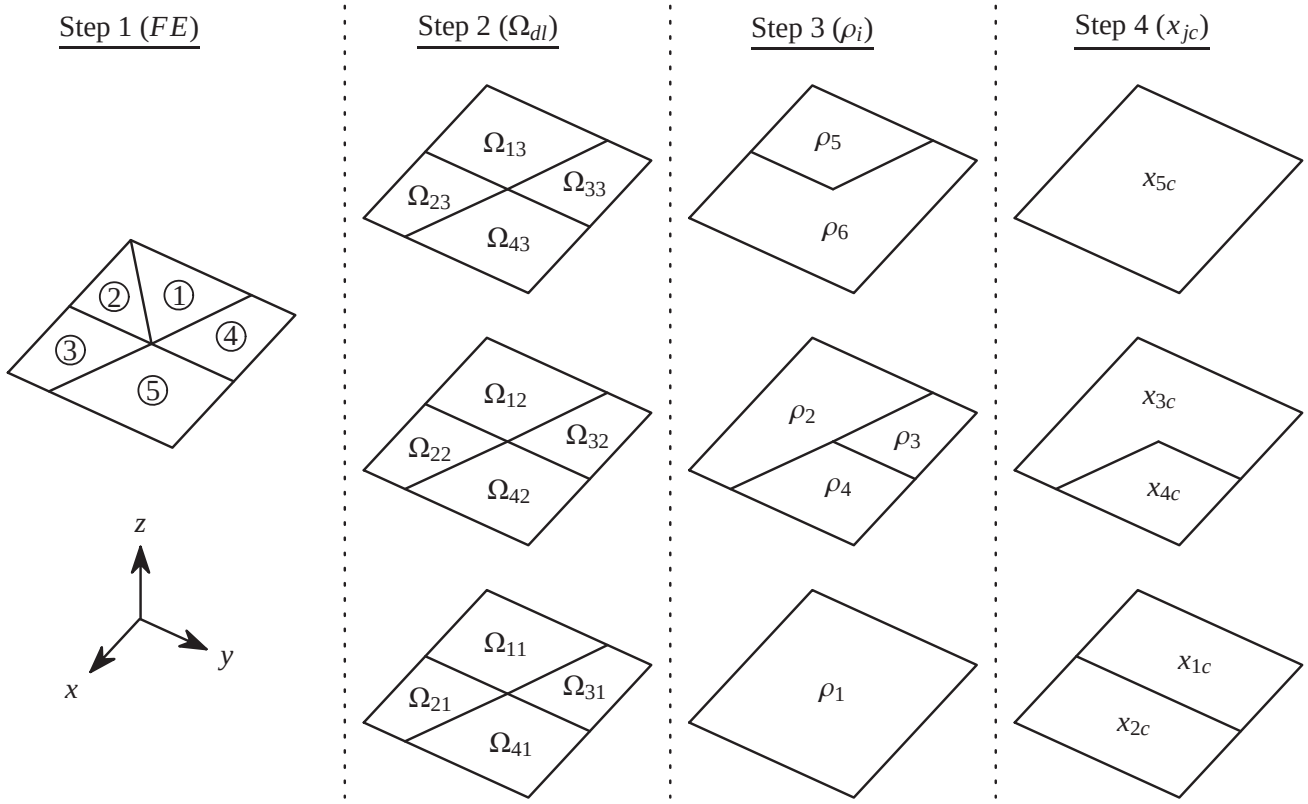

Figure 1: The design parameterization takes place in 4 steps. Step 1 concerns the finite element discretization. Step 2 concerns the arrangement into sub-domains, Ω_{dl}. Step 3 and Step 4 concern the parameterizations into geometry domains, ρ_i, and candidate domains, x_{jc}, respectively

2 The DMTO method

2.1 Design parameterization

Out of generality, this work clearly distinguishes between the initial finite element discretization and following arrangement into domains limiting the complexity of the geometric outcome, and domains limiting the complexity of the possible candidate distribution. As the results in Section 4 will demonstrate, the design parameterization significantly affects both performance and complexity of the optimized designs. The designer must from the very beginning keep in mind that the design parameterization should reflect adequate limits of complexity in manufacturing, thereby making it possible to realize the optimized design given an acceptable level of post-processing. The design parameterization takes place in four steps as exemplified in Fig. 1. Step 1 of Fig. 1 concerns the finite element (FE) discretization into an appropriate number of Equivalent Single Layer (ESL) shell elements all with an identical number of layers of uniform thickness. In the figure, five elements are shown, each having three layers of uniform thickness. The appropriate number of elements may be determined based on a convergence study, considering all optimization criteria. The necessary finite element discretization may, however, often be too fine for the acceptable level of the thickness variation and transitions in fiber orientation or different material selection that is about to take place. This problem is considered in Step 2, where the designer must settle on a sufficiently detailed level for such variations and transitions, common for all layers.

Hence, Step 2 concerns the arrangement of finite elements into a number of sub-domains Ω_{dl}, which are identically shaped for all layers covered by the sub-domain, where indices $d = 1, 2, \ldots, n^d$ and $l = 1, 2, \ldots, n^l$ denote sub-domain number and layer number, respectively. Consequently, the sub-domains are coincident with the boundaries of at least one of the finite elements and do not overlap each other. The sub-domains constitute the building blocks for the subsequent parameterization into domains that are directly associated with the design variables. For this illustrative example, finite elements 1 and 2 have been collapsed into the sub-domain $d = 1$, and the remaining elements have been assigned as sub-domains $d = \{2, 3, 4\}$.

Step 3 concerns the adequate parameterization for the laminate thickness variation. For this purpose we introduce the so-called topology variables $\rho_i \in [0, 1]$ with the desirable limit value interpretation

$$\rho_i = \begin{cases} 1 & \text{if there is material in geometry domain } i \\ 0 & \text{otherwise} \end{cases} \tag{1}$$

where the index $i = 1, 2, \ldots, n^i$ denotes the so-called geometry domain number. The geometry domains are coincident with the boundaries of at least one of the sub-domains. The geometry domains may principally overlap each other from layer to layer as seen in Fig. 1; it is up

to the manufacturing constraints to ensure e.g., prevention of intermediate void. Application of a single topology variable for the bottom layer $l = 1$ ensures a constant thickness throughout governed by the value of ρ_1.

In Step 4, the acceptable level for jointing adjacent fiber mats with different orientations, different biax-angle plies, NCF's, or even different materials, is defined. For this purpose we introduce the so-called candidate variables $x_{jc} \in [0, 1]$ with the desirable limit value interpretation

$$x_{jc} = \begin{cases} 1 & \text{if cand. } c \text{ is chosen in cand. domain } j \\ 0 & \text{otherwise} \end{cases} \tag{2}$$

where index $j = 1, 2, \ldots, n^j$ denotes the so-called candidate domain number and index $c = 1, 2, \ldots, n^c$ denotes the candidate number. A candidate c represents a unique set of material properties for the constitutive tensor $\boldsymbol{E}_c \in \mathbb{R}^{6\times6}$. Hence, some candidates may represent differently oriented UniDirectional (UD) fiber mats, while other candidates may represent biax-angle plies, NCF's, or isotropic materials such as a lightweight foam in case of designing sandwich structures. Hence, the method supports any set of physical constitutive properties. Similar to the geometry domains ρ_i, the candidate domains x_{jc} may likewise overlap each other from layer to layer as seen in Fig. 1.

Figure 2 illustrates a potential outcome of the considered example where the constitutive properties characterizing a Glass Fiber Reinforced Polymer (GFRP) $\pm45°$ biax-angle ply represents the material candidate $c = 1$ and hence $\boldsymbol{E}_1$, an isotropic foam material represents candidate $c = 2$ ($\boldsymbol{E}_2$), and a UD GFRP oriented at $-45°$ represents candidate $c = 3$ ($\boldsymbol{E}_3$). The design parameterization of Fig. 1 and the outcome illustrated in Fig. 2 are used to exemplify the formulation and effect of certain manufacturing constraints in succeeding sections. Presence of exactly one candidate must naturally ensure absence of remaining ones. In this work we ensure this coherence explicitly through the series of linear equality constraints

$$\sum_{c=1}^{n^c} x_{jc} = 1 \quad \forall\ j \tag{3}$$

It is noticed that (3) is of no importance for obtaining the desirable $0/1$ designs; this is left for penalization of intermediate values through the density approach.

2.2 Density approach

The constraints (3) in combination with continuous candidate variables introduce the risk of non-manufacturable, non-physical pseudo candidates if linearly summarized to describe the effective constitutive properties $\boldsymbol{E}_{el}$ for all layers of all elements e as

$$\boldsymbol{E}_{el} = \sum_{c=1}^{n^c} x_{jc} \boldsymbol{E}_c \tag{4}$$

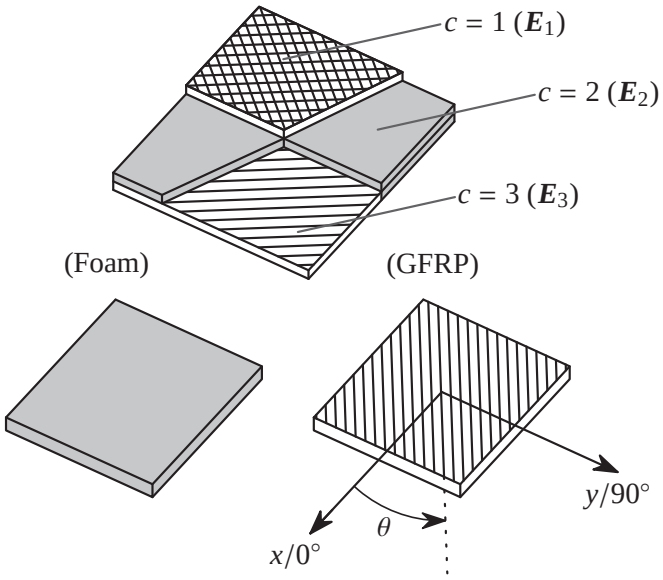

Figure 2: *Top:* Potential outcome of an example, parameterized as illustrated in Fig. 1. *Bottom:* Any unique set of material properties for the constitutive tensor $\boldsymbol{E}_c$ may represent a candidate c such as for instance a foam type (left) or GFRP UD fiber mats (right), characterized by the fiber orientation θ

In (4), careful bookkeeping keeps track of proper association between finite element discretization versus design variable location. We introduce a product of RAMP interpolation schemes to facilitate difference in geometric variation and candidate distribution while making binary variables attractive.

$$\boldsymbol{E}_{el} = \boldsymbol{E}_0 + \frac{\rho_i}{1 + p(1-\rho_i)} \sum_{c=1}^{n^c} \frac{x_{jc}}{1 + p(1-x_{jc})} \Delta\boldsymbol{E}_c \tag{5}$$

where $\Delta\boldsymbol{E}_c = \boldsymbol{E}_c - \boldsymbol{E}_0$ with $\boldsymbol{E}_0$ representing void such that $\boldsymbol{E}_c - \boldsymbol{E}_0 \succ 0$ and $\boldsymbol{E}_0 \succ 0$. In (5), $p \geq 0.0$ is a penalization power. Notice that variables ρ_i and x_{jc} are subject to identical penalization, found appropriate by experience. We favor the RAMP interpolation scheme by Stolpe and Svanberg (2001) after Rietz (2001) because of non-zero sensitivities even for zero valued design variables for all penalization powers. Other schemes exist and are known to work as well; it is a matter of preference. Equivalent penalization between the RAMP scheme and the well-known SIMP scheme by Bendsøe (1989) is treated in Hvejsel and Lund (2011).

Notice that the products $\rho_i x_{jc}$ ensure candidate continuity within the pre-defined candidate domains while having the freedom to introduce regions with void through topology variable scaling. This facilitates an outcome as illustrated in Fig. 2, subject to the parameterization of Fig. 1. Here, the candidate domain x_{5c}, covering sub-domains $\{\Omega_{13}, \Omega_{23}, \Omega_{33}, \Omega_{43}\}$, has settled on the specific biax-angle candidate $c = 1$, but since the topology variable $\rho_6 = 0$, only sub-domain Ω_{13} where $\rho_5 = 1$ appears. The association between sub-domains Ω_{dl}, geometry do-

mains ρ_i, candidate domains x_{jc}, and the corresponding design variable value distribution for the considered example in Fig. 2 appears in (6) in case the number of candidates is limited to those three introduced in Fig. 2 (top), i.e., $n^c = 3$.

$$\begin{bmatrix} \Omega_{11} \\ \Omega_{12} \\ \Omega_{13} \\ \hline \Omega_{21} \\ \Omega_{22} \\ \Omega_{23} \\ \hline \Omega_{31} \\ \Omega_{32} \\ \Omega_{33} \\ \hline \Omega_{41} \\ \Omega_{42} \\ \Omega_{43} \end{bmatrix} \longleftrightarrow \begin{bmatrix} \rho_1 = 1 \\ \rho_2 = 1 \\ \rho_5 = 1 \\ \hline \rho_1 = 1 \\ \rho_2 = 1 \\ \rho_6 = 0 \\ \hline \rho_1 = 1 \\ \rho_3 = 1 \\ \rho_6 = 0 \\ \hline \rho_1 = 1 \\ \rho_4 = 0 \\ \rho_6 = 0 \end{bmatrix} \longleftrightarrow \begin{bmatrix} x_{1c} = \{ \ 0 \ 1 \ 0 \ \} \\ x_{3c} = \{ \ 0 \ 1 \ 0 \ \} \\ x_{5c} = \{ \ 1 \ 0 \ 0 \ \} \\ \hline x_{2c} = \{ \ 0 \ 0 \ 1 \ \} \\ x_{3c} = \{ \ 0 \ 1 \ 0 \ \} \\ x_{5c} = \{ \ 1 \ 0 \ 0 \ \} \\ \hline x_{1c} = \{ \ 0 \ 1 \ 0 \ \} \\ x_{3c} = \{ \ 0 \ 1 \ 0 \ \} \\ x_{5c} = \{ \ 1 \ 0 \ 0 \ \} \\ \hline x_{2c} = \{ \ 0 \ 0 \ 1 \ \} \\ x^*_{4c} = \{ \ 1 \ 0 \ 0 \ \} \\ x_{5c} = \{ \ 1 \ 0 \ 0 \ \} \end{bmatrix} \tag{6}$$

The star on x^*_{4c} denotes that the candidate material selection in this particular case is insignificant because the associated geometry domain is empty, i.e., $\rho_4 = 0$. The design variable value distribution for x^*_{4c} must comply with (3) but could as such be $x^*_{4c} = \left\{ \ \frac{1}{3} \ \frac{1}{3} \ \frac{1}{3} \ \right\}$ or any other combination with no influence on the effective constitutive properties, given (5) with $\rho_4 = 0$.

With the stiffness parameterization (5), one could likewise determine how, for instance, the well-known Messerschmitt-Bølkow-Blohm (MBB) beam, see e.g., Olhoff et al. (1991) or Bendsøe and Sigmund (2003), would appear, if the entire domain should settle on a specific candidate from a distinct set while having the possibility to mix with void through topology variable scaling. The outcome would indeed be quite easily manufacturable.

An approach as (5) where stiffness is determined through interpolation schemes with penalization, but mass is not, making non 0/1 variable values uneconomical, is generally referred to as the density approach, and is used extensively throughout the literature on structural topology optimization, see Bendsøe and Sigmund (2003). The density approach is known to work particularly well for mass constrained minimization of compliance, but may nevertheless fail at obtaining pure 0/1 designs for various reasons. The difficulties of obtaining binary designs are increased in this work, primarily due to the presence of sensitivities with both operational signs. For this reason, we finalize the optimized designs with simple rounding to binary values, elaborated in Section 2.6. To assess the quality of the optimized designs prior to this rounding, we will introduce so-called measures of non-discreteness in Section 2.5. The finite element formulations of the considered criteria functions are treated in Section 2.4.

2.3 Manufacturing constraints

Practical design guidelines or rules, referred to as manufacturing constraints in this work, occur frequently in the literature. As described in the introduction, manufacturing constraints are typically associated with different out-of-plane failure modes and may be implemented in various ways. In this work, we explicitly include a variety of manufacturing constraints as linear inequalities to accommodate demands on manufacturability. The linear formulations are highly attractive and possible to achieve for most manufacturing constraints. Explicit inclusion from the very beginning is the key to the simultaneous determination of geometry, i.e., the variation in thickness, *and* the proper candidate choice from a predefined, distinct set. Formulations of the manufacturing constraints are deemed most easily comprehensible when exemplified as below with basis in the parameterization presented in Fig. 1 and the resulting outcome in Fig. 2. Correct formulation relies on proper bookkeeping between the parameterizations applied in Steps 2 – 4, exemplified in (6) for the outcome in Fig. 2.

2.3.1 Accommodations for allowable candidate and thickness variation (MC1)

MC1 concerns the possible arrangement or grouping of small finite element domains into larger domains, adequate for the allowable variation in both candidate selection and thickness. These latter domains are directly associated with the design variables as part of the design parameterization, see Steps 3-4 in Fig. 1. It is thus possible to e.g., ensure sufficiently large areas with identical candidate selection to support standard roll widths for fibrous material. Hence, MC1 reflects adequate limits of complexity with regards to the available production methods, thereby making it possible to realize the optimized designs with quite little post-processing.

2.3.2 Constraints on thickness variation rate (MC2)

Let $S \in \mathbb{N}$ denote the allowable difference in the total number of plies between adjacent geometry domains, ρ_i. Constraints to govern the acceptable thickness variation rate e-merge on basis of systematical comparison between topology variable summation through the thickness of all adjacent design domains Ω_{dl}, taking into account, however, possible reduction because certain topology variable pairs may cancel out each other, caused by the fact that geometry domains can overlap several sub-domains. This gives rise to four linear inequalities for the considered example.

$\underline{\Omega_{1l} \text{ vs } \Omega_{2l}:}$

$$-S \leq (\cancel{\rho_1} + \cancel{\rho_2} + \rho_5) - (\cancel{\rho_1} + \cancel{\rho_2} + \rho_6) \leq S \tag{7a}$$

Ω_{1l} vs Ω_{3l} :

$$-S \leq (\cancel{\rho_1} + \rho_2 + \rho_5) - (\cancel{\rho_1} + \rho_3 + \rho_6) \leq S \tag{7b}$$

Ω_{2l} vs Ω_{4l} :

$$-S \leq (\cancel{\rho_1} + \rho_2 + \cancel{\rho_6}) - (\cancel{\rho_1} + \rho_4 + \cancel{\rho_6}) \leq S \tag{7c}$$

Ω_{3l} vs Ω_{4l} :

$$-S \leq (\cancel{\rho_1} + \rho_3 + \cancel{\rho_6}) - (\cancel{\rho_1} + \rho_4 + \cancel{\rho_6}) \leq S \tag{7d}$$

The outcome in Fig. 2 is feasible for all $S \geq 1$.

2.3.3 Constraints on contiguity (MC3)

Let $\mathcal{P}^c_{(UD)}$ denote the unique set of indices c that concerns UD fiber material candidates. The constraints on contiguity impose a limit on the maximum allowable number of contiguous identical UD fiber material candidates to avoid e.g., matrix cracking failure. Hence, non UD candidates are not subject to the following constraints. Let $CL \in \mathbb{N}$ denote the contiguity limit. In case $CL = 1$, the candidate selection for all contiguous Ω_{dl} pairs must be constrained. However, since the candidate domains are larger than or equal to the sub-domains, we see that a number of constraints repeat themselves for which reason the redundant ones are erased for efficiency.

Concerning Ω_{1l} :

$$x_{1c} + x_{3c} \leq CL \quad \forall c \in \mathcal{P}^c_{(UD)} \tag{8a}$$
$$x_{3c} + x_{5c} \leq CL \quad \forall c \in \mathcal{P}^c_{(UD)} \tag{8b}$$

Concerning Ω_{2l} :

$$x_{2c} + x_{3c} \leq CL \quad \forall c \in \mathcal{P}^c_{(UD)} \tag{8c}$$
$$\cancel{x_{3c} + x_{5c} \leq CL \quad \forall c \in \mathcal{P}^c_{(UD)}} \tag{8d}$$

Concerning Ω_{3l} :

$$\cancel{x_{1c} + x_{3c} \leq CL \quad \forall c \in \mathcal{P}^c_{(UD)}} \tag{8e}$$
$$\cancel{x_{3c} + x_{5c} \leq CL \quad \forall c \in \mathcal{P}^c_{(UD)}} \tag{8f}$$

Concerning Ω_{4l} :

$$x_{2c} + x_{4c} \leq CL \quad \forall c \in \mathcal{P}^c_{(UD)} \tag{8g}$$
$$x_{4c} + x_{5c} \leq CL \quad \forall c \in \mathcal{P}^c_{(UD)} \tag{8h}$$

For the example in Fig. 2, only $c = 3$ is a UD fiber material candidate; hence $\mathcal{P}^c_{(UD)} = \{3\}$.

2.3.4 Preventing intermediate void (MC4)

Intermediate void must be prevented in order to support common manufacturing techniques relying on vacuum infusion. To facilitate this, it principally suffices to ensure that topology variable values of upper layers do not exceed those of lower contiguous layers such as for instance $\rho_5 \leq \rho_2 \leq \rho_1$, see Fig. 1. In the preceding work by Sørensen and Lund (2013) it was, however, concluded that series of such straightforward constraints were insufficient at preventing so-called density bands where the topology variables settled on the same intermediate value throughout the thickness regardless of the penalization level. For this reason we apply the same modified constraints to prevent intermediate void as suggested in Sørensen and Lund (2013), thereby ensuring an acceptable transition between contiguous topology variables throughout the thickness. The constraints emerge systematically on basis of the sub-domain arrangement Ω_{dl} followed by removal of repeated constraints because of potentially larger geometry domains ρ_i. This gives rise to seven linear inequalities for the considered example.

Concerning Ω_{1l} :

$$\rho_2 \leq f(\rho_1, T) \tag{9a}$$
$$\rho_5 \leq f(\rho_2, T) \tag{9b}$$

Concerning Ω_{2l} :

$$\cancel{\rho_2 \leq f(\rho_1, T)} \tag{9c}$$
$$\rho_6 \leq f(\rho_2, T) \tag{9d}$$

Concerning Ω_{3l} :

$$\rho_3 \leq f(\rho_1, T) \tag{9e}$$
$$\rho_6 \leq f(\rho_3, T) \tag{9f}$$

Concerning Ω_{4l} :

$$\rho_4 \leq f(\rho_1, T) \tag{9g}$$
$$\rho_6 \leq f(\rho_4, T) \tag{9h}$$

In (9) the right-hand sides $f(\rho_i, T)$ denote functions depending upon density values of contiguous lower layers and a threshold value T to control the transition, given as

$$f(\rho_i, T) = \begin{cases} \frac{T}{1-T}\rho_i & \text{if} \quad \rho_i < (1-T) \\ \frac{1-T}{T}\rho_i + \frac{2T-1}{T} & \text{else} \end{cases} \tag{10}$$

In Sørensen and Lund (2013), the threshold value $T = 0.10$ was found appropriate and is used in this work as well. Because the topology variable $\rho_4 = 0$ for the example in Fig. 2, ρ_6 must likewise be equal to zero to fulfill (9h), thereby efficiently preventing intermediate void.

2.4 Mathematical formulation of the optimization problem

In this work, we want to minimize the total mass, subject to constraints on buckling load factors, eigenfrequencies, displacements, and the linear manufacturing constraints presented in Section 2.3. We apply the Nested

ANalysis and Design (NAND) approach, see for instance Arora and Wang (2005), to solve the optimization problem that appears in (11).

$$\min_{\rho_i, x_{jc}} \quad m \qquad (Mass) \tag{11a}$$

$$\text{s.t.} \quad \lambda_k^{(b)} \geq \underline{\lambda}^{(b)} \; k = 1, 2, \ldots, n_\lambda^{(b)} \qquad (Buck) \tag{11b}$$

$$\lambda_k^{(f)} \geq \underline{\lambda}^{(f)} \; k = 1, 2, \ldots, n_\lambda^{(f)} \qquad (Freq) \tag{11c}$$

$$|u_o| \leq \overline{u}_o \quad \forall o \in \mathcal{P}^u \qquad (Disp) \tag{11d}$$

$$(\text{MC's}) \tag{11e}$$

$$\rho_i \in [0, 1] \;\; \forall \; i \tag{11f}$$

$$x_{jc} \in [0, 1] \forall \; (j, c) \tag{11g}$$

In (11a), m denotes the total mass, determined as

$$m = \sum_{d,l} \rho_i V_{dl} \sum_{c=1}^{n^c} x_{jc} \varrho_c \tag{12}$$

taking into account proper association between indices dl, i, and j, as exemplified in (6). V_{dl} denotes the volume of sub-domain Ω_{dl}, and ϱ_c is the material density of candidate c. In (11b), $\underline{\lambda}^{(b)}$ denotes the minimum allowable buckling load factor. $\lambda_k^{(b)}$ denotes the k^{th} eigenvalue, i.e., buckling load factor, out of the considered $n_\lambda^{(b)}$ eigenvalues, assumed ordered by magnitude such that $\lambda_1^{(b)}$ is the lowest positive eigenvalue. The advantage of including $n_\lambda^{(b)}$ and $n_\lambda^{(f)}$ eigenvalues in the optimization problem instead of only including the lowest eigenvalue is that crossing eigenvalues (mode switching) during the optimization process are taken into account. In the examples considered the lowest 10 buckling load factors and eigenfrequencies are included. Based on the displacement field, the stress stiffening effects due to the mechanical loading can be evaluated by computing the initial stress stiffness matrix, also termed the geometric stiffness matrix, $\boldsymbol{K}_\sigma$, and the linearized buckling problem can be established as

$$\left(\boldsymbol{K}_0 + \lambda_k^{(b)} \boldsymbol{K}_\sigma\right) \boldsymbol{\Phi}_k^{(b)} = \boldsymbol{0} \,, \quad k = 1, 2, \ldots, n_\lambda^{(b)} \tag{13}$$

where $\boldsymbol{\Phi}_k^{(b)}$ denotes the corresponding eigenvector of displacements and $\boldsymbol{K}_0$ is the linear stiffness matrix. The notation in (11c) is similar but with superscript (f) denoting frequency. Hence, $\omega_k^2 = \lambda_k^{(f)}$ is the k^{th} squared, undamped, free, natural eigenfrequency, determined from the free vibration analysis problem

$$\left(\boldsymbol{K}_0 - \lambda_k^{(f)} \boldsymbol{M}\right) \boldsymbol{\Phi}_k^{(f)} = \boldsymbol{0} \,, \quad k = 1, 2, \ldots, n_\lambda^{(f)} \tag{14}$$

where $\boldsymbol{\Phi}_k^{(f)}$ denotes the corresponding eigenvector, i.e., nodal amplitudes, and $\boldsymbol{M}$ is the consistent global mass matrix. Eigenvalues are again assumed ordered by magnitude. In (11d), $|u_o|$ denotes the absolute displacement of the nodal degree of freedom (DOF) o, constrained by a maximum allowable displacement $\overline{u}_o$. Elastic couplings may necessitate displacement constraints on several nodal DOF's, contained in a corresponding set, denoted by $\mathcal{P}^u$. Given the NAND approach, the global displacement vector $\boldsymbol{u}$ is determined prior to every optimization iteration from the static equilibrium equations

$$\boldsymbol{K}_0 \boldsymbol{u} = \boldsymbol{f} \tag{15}$$

written in residual form as

$$\boldsymbol{r}(\boldsymbol{u}, \rho_i, x_{jc}) = \boldsymbol{K}_0 \boldsymbol{u} - \boldsymbol{f} = \boldsymbol{0} \tag{16}$$

where $\boldsymbol{f}$ denotes the load applied to the non-restrained nodes and $\boldsymbol{r}$ is the residual. Besides the total mass m in (12) that is clearly a function of the design variables ρ_i and x_{jc}, it must by now be noticed that this is likewise the case for both $\boldsymbol{K}_0$ and $\boldsymbol{K}_\sigma$ due to the dependence on the effective constitutive properties (5). It is neither trivial nor obvious where to most efficiently penalize this design variable dependence. In this work, however, we reserve penalization p for the linear stiffness matrix part $\boldsymbol{K}_0$ only, i.e.,

$$\boldsymbol{K}_0 = f(p) \quad , \quad \boldsymbol{K}_\sigma \neq f(p) \quad , \quad m \neq f(p) \tag{17}$$

The numerical results in Section 4 will demonstrate the efficiency of this approach, and alternative penalization is left for future work. See for instance Lindgaard and Dahl (2012) for penalization approaches concerning topology optimization of geometric non-linear compliance and buckling.

2.4.1 Design sensitivity analysis

Let z_i represent all design variables ρ_i and x_{jc} in the following, where the index $i = 1, 2, \ldots, n^i n^j n^c$. This subsection describes how we conduct analytical, computationally efficient adjoint Design Sensitivity Analysis (DSA) of displacements, $\frac{d\boldsymbol{u}}{dz_i}$, and distinct eigenvalues, $\frac{d\lambda_k^{(f)}}{dz_i}$ and $\frac{d\lambda_k^{(b)}}{dz_i}$, concerning eigenfrequencies and buckling load factors, respectively. Notice that this work is limited to DSA of distinct eigenvalues as opposed to the more complicated case where two or several eigenvalues attain exactly the same value, known as repeated or multiple eigenvalues. For details on this latter case see e.g., Seyranian et al. (1994) or Lund (1994). DSA of the objective function mass in (12), $\frac{dm}{dz_i}$, is straightforward and omitted.

The displacement sensitivities $\frac{d\boldsymbol{u}}{dz_i}$ can be computed using the direct differentiation approach, i.e., the static equilibrium equations (15) are differentiated with respect to a design variable z_i as

$$\boldsymbol{K}_0 \frac{d\boldsymbol{u}}{dz_i} = \frac{\partial \boldsymbol{f}}{\partial z_i} - \frac{\partial \boldsymbol{K}_0}{\partial z_i} \boldsymbol{u} \tag{18}$$

where the load sensitivities $\partial \boldsymbol{f}/\partial z_i$ are zero for the DMTO design variables used, unless volume forces are considered which is not the case in this work. (18) is written alternatively in residual form as

$$\frac{d\boldsymbol{u}}{dz_i} = -\boldsymbol{K}_0^{-1}\frac{\partial \boldsymbol{r}}{\partial z_i} \tag{19}$$

For the DMTO parameterization proposed in this work, the design domain is fixed. For this reason the derivative $\frac{\partial \boldsymbol{K}_0(z_i)}{\partial z_i}$ in the pseudo load vector $\frac{\partial \boldsymbol{r}}{\partial z_i}$ involves only the derivative of the assembled effective constitute element matrix $\boldsymbol{E}_e$, which is determined analytically. However, the DMTO parameterization introduces many design variables, and it is thus more efficient to compute the displacement sensitivity using the adjoint method. Noting that the displacement u_o can be expressed as $u_o = \boldsymbol{l}^T\boldsymbol{u}$, where $\boldsymbol{l}$ is a vector with the value 1 at the DOF of interest, the sensitivity of the displacement u_o can be found analytically as

$$\frac{du_o}{dz_i} = -\boldsymbol{w}^T\frac{\partial \boldsymbol{r}}{\partial z_i} \tag{20}$$

where the vector $\boldsymbol{w}$ is the solution to the adjoint load problem

$$\boldsymbol{K}_0\boldsymbol{w} = \boldsymbol{l} \tag{21}$$

In this way, the factored stiffness matrix $\boldsymbol{K}_0$ is reused and only a single forward/backward substitution is needed for each displacement constraint u_o before the displacement sensitivities in (20) are obtained analytically by vector multiplications.

The direct approach to obtain the eigenfrequency sensitivity is to differentiate (14) with respect to a design variable z_i, premultiply by $\left(\boldsymbol{\Phi}_k^{(f)}\right)^T$, make use of (14), and noting that the system matrices are symmetric. Hence the following expression is obtained for the eigenvalue sensitivity in case of a simple, i.e., distinct, eigenvalue λ_j, see e.g., Courant and Hilbert (1953) and Wittrick (1962).

$$\frac{d\lambda_k^{(f)}}{dz_i} = \left(\boldsymbol{\Phi}_k^{(f)}\right)^T\left(\frac{d\boldsymbol{K}_0}{dz_i} - \lambda_j^{(f)}\frac{d\boldsymbol{M}}{dz_i}\right)\boldsymbol{\Phi}_k^{(f)} \tag{22}$$

Here it is assumed that the eigenvectors have been $\boldsymbol{M}$-orthonormalized such that $\left(\boldsymbol{\Phi}_k^{(f)}\right)^T\boldsymbol{M}\boldsymbol{\Phi}_k^{(f)} = 1$. Again, the derivatives $\frac{d\boldsymbol{K}_0(z_i)}{dz_i}$ and $\frac{d\boldsymbol{M}(z_i)}{dz_i}$ are computed analytically, as they involve only the derivative of the assembled effective constitute matrix $\boldsymbol{E}_e$ and the material candidate mass density ϱ_c with respect to z_i. Note that in a finite element implementation, all of these computations are performed on the element level, such that derivatives are only computed for elements depending on the given design variable z_i.

In a similar way the design sensitivity of a distinct buckling load factor is given as

$$\frac{d\lambda_k^{(b)}}{dz_i} = \left(\boldsymbol{\Phi}_k^{(b)}\right)^T\left(\frac{d\boldsymbol{K}_0}{dz_i} + \lambda_k^{(b)}\frac{d\boldsymbol{K}_\sigma}{dz_i}\right)\boldsymbol{\Phi}_k^{(b)} \tag{23}$$

where the eigenvectors have been $\boldsymbol{K}_\sigma$-orthonormalized, such that $\left(\boldsymbol{\Phi}_k^{(b)}\right)^T(-\boldsymbol{K}_\sigma)\boldsymbol{\Phi}_k^{(b)} = 1$. The first of the derivatives $\frac{d\boldsymbol{K}_0(z_i)}{dz_i}$ is computed analytically as described before, but the second term $\frac{d\boldsymbol{K}_\sigma(z_i)}{dz_i}$ in (23) is more complicated because of the implicit dependence of the state variables $\boldsymbol{u}$, i.e., $\boldsymbol{K}_\sigma(z_i, \boldsymbol{u}(z_i))$. In this work an efficient analytical adjoint method is introduced due to the many design variables in the DMTO approach. The adjoint method is based on the work presented in Rodrigues et al. (1995) and Neves et al. (1995), but is nevertheless described here for completeness. Applying the chain rule we have

$$\frac{d\boldsymbol{K}_\sigma(z_i, \boldsymbol{u}(z_i))}{dz_i} = \frac{\partial \boldsymbol{K}_\sigma(z_i, \boldsymbol{u})}{\partial z_i} + \frac{\partial \boldsymbol{K}_\sigma(z_i, \boldsymbol{u})}{\partial \boldsymbol{u}}\frac{d\boldsymbol{u}}{dz_i} \tag{24}$$

Again, the first term is the partial derivative of $\boldsymbol{K}_\sigma$ and this term is computed on the element level in the same way as described for the term $\frac{d\boldsymbol{K}_0(z_i)}{dz_i}$. The second term of (24) involving $\partial \boldsymbol{K}_\sigma/\partial \boldsymbol{u}$ is the difficult and costly part to compute and still requires evaluation of state variable sensitivities $d\boldsymbol{u}/dz_i$ for all design variables. However, note that we are not *really* interested in computing the term, but instead it is to be pre- and post-multiplied with some eigenvectors in (23), i.e.,

$$\begin{aligned}&\left(\boldsymbol{\Phi}_k^{(b)}\right)^T\frac{\partial \boldsymbol{K}_\sigma(z_i, \boldsymbol{u})}{\partial \boldsymbol{u}}\frac{d\boldsymbol{u}}{dz_i}\boldsymbol{\Phi}_k^{(b)} = \dots \\ &\dots - \left(\boldsymbol{\Phi}_k^{(b)}\right)^T\frac{\partial \boldsymbol{K}_\sigma(z_i, \boldsymbol{u})}{\partial \boldsymbol{u}}\boldsymbol{\Phi}_k^{(b)}\boldsymbol{K}_0^{-1}\frac{\partial \boldsymbol{r}}{\partial z_i}\end{aligned} \tag{25}$$

where the right hand side is arrived at by inserting the expression for state sensitivities $d\boldsymbol{u}/dz_i$ from (19) and regrouping terms exploiting symmetries. It is now convenient to introduce the adjoint vectors $\boldsymbol{v}_{kk}$ given as

$$\boldsymbol{v}_{kk}^T = \left(\boldsymbol{\Phi}_k^{(b)}\right)^T\frac{\partial \boldsymbol{K}_\sigma(z_i, \boldsymbol{u})}{\partial \boldsymbol{u}}\boldsymbol{\Phi}_k^{(b)}\boldsymbol{K}_0^{-1} \tag{26}$$

Notice that $\boldsymbol{v}_{kk}$ is the same for all design variables, and thus only needs to be computed once for each iteration of the optimization problem for each of the $n_\lambda^{(b)}$ buckling load factors included in the optimization problem (11). When solving the linear systems of equations in (26) for the adjoint vector $\boldsymbol{v}_{kk}$, the factored stiffness matrix $\boldsymbol{K}_0$ can be reused. The term $\partial \boldsymbol{K}_\sigma/\partial \boldsymbol{u}$ is derived analytically for the ESL shell elements used, and by using (26) and (24) in (23) and regrouping terms, the buckling load factor sensitivity can be computed analytically as

$$\begin{aligned}\frac{d\lambda_k^{(b)}}{dz_i} &= \left(\boldsymbol{\Phi}_k^{(b)}\right)^T\frac{d\boldsymbol{K}_0}{dz_i}\boldsymbol{\Phi}_k^{(b)} + \dots \\ &\dots \lambda_k^{(b)}\left(\left(\boldsymbol{\Phi}_k^{(b)}\right)^T\frac{\partial \boldsymbol{K}_\sigma(z_i, \boldsymbol{u}(z_i))}{\partial z_i}\boldsymbol{\Phi}_k - \boldsymbol{v}_{kk}^T\frac{\partial \boldsymbol{r}}{\partial z_i}\right)\end{aligned} \tag{27}$$

In this way the sensitivities of the buckling load factors are computed very efficiently. The described DSA requires full access to the finite element code used in order to implement analytical sensitivities of element matrices and vectors, and for implementation of the term $\partial \boldsymbol{K}_\sigma/\partial \boldsymbol{u}$ needed for computing adjoint vectors in the analytical DSA of buckling load factors.

2.5 The SLP approach

Previous work by Sørensen and Lund (2013) concluded that an SLP approach outperformed various Sequential Quadratic Programming (SQP) approaches, primarily due to the nature of the manufacturing constraints to prevent intermediate void through the laminate thickness, i.e., MC4 from (10). As this work includes the same challenging manufacturing constraints, we rely on an SLP approach once more, see for instance Arora (2004). The complexity of this work does, however, surpass that of Sørensen and Lund (2013) given the presence of several non-linear structural constraints. Hence, in order to pose unconditionally feasible linearized programming problems, we introduce an elastic programming technique with merit functions.

2.5.1 Introduction of merit functions

Merit functions $\Phi_M^{(n)} = f(x_{jc}^{(n)}, \rho_i^{(n)}, y_k^{(n)})$, where the superscript (n) denotes the iteration number and $M = 1 + K$ denotes an objective function and K non-linear structural inequalities, are introduced to ensure feasibility of all linearized optimization problems. Inspired by Svanberg's work on the Method of Moving Asymptotes (MMA), see e.g., Svanberg (1987), we introduce the objective merit function

$$\Phi_0^{(n)} = m^{(n)} + a \sum_{k=1}^{K} \left(c y_k^{(n)} + \frac{1}{2} \left(y_k^{(n)} \right)^2 \right) \tag{28}$$

where $m^{(n)} = f(x_{jc}^{(n)}, \rho_i^{(n)})$ is the original objective function, $x_{jc}^{(n)}$ and $\rho_i^{(n)}$ are the true optimization variables, while $y_k^{(n)} \in [0.0, \infty[$ are artificial optimization variables, also known as slack variables, that are subtracted the structural non-linear inequality constraints $g_k^{(n)} = f(x_{jc}^{(n)}, \rho_i^{(n)})$, resulting in the constraint merit functions

$$\Phi_k^{(n)} = g_k^{(n)} - y_k^{(n)} \leq g_k^{\max} \quad , \quad k = 1, 2, \ldots, K \tag{29}$$

that in combination with (28) ensure feasibility of the non-linear structural constraints. In (28), c is a positive penalization constant ensuring that the artificial variables $y_k^{(n)}$ become expensive when larger than the desired zero values. In agreement with the practical considerations and recommendations in Svanberg (2004), all non-linear constraints are normalized with respect to $g_k^{\max}$, c is initially set to 100.0, and the constant a is set to $m^{(1)}$, serving the purpose of proper scaling between the objective function and the non-linear constraints. With the introduction of (28) and (29), the optimization problem which is to be linearized and solved sequentially in a number of iterations by an efficient LP optimizer is now defined as

$$\min_{\rho_i, x_{jc}, y_k} \quad \Phi_0^{(n)} \tag{30a}$$

$$\text{s.t.} \quad \Phi_k^{(n)} \leq g_k^{\max} \qquad k = 1, 2, \ldots, K \tag{30b}$$

$$\text{(MC's)} \tag{30c}$$

$$\rho_i^{(n)} \in ML \qquad \forall\, i \tag{30d}$$

$$x_{jc}^{(n)} \in ML \qquad \forall\, (j, c) \tag{30e}$$

$$y_k^{(n)} \in [0, \infty[\qquad \forall\, k \tag{30f}$$

In (30d) and (30e), the set ML refers to the bounds of the design variables which may change in each iteration due to the applied move limit strategy, described in the following subsection. Notice that feasibility of the linear manufacturing constraints can only be guaranteed if the initial linear problem is feasible, and if the move limits ML repeatedly include the previous design point.

2.5.2 Move limit strategy

Without precautions, any SLP approach is inherently subject to oscillating function and design variable values. Hence, a robust move limit strategy must be applied. In this work, surveillance of a merit function is used to deem the validity range of the linearizations. An oscillating merit function suggests that move limits should be reduced, whereas monotonous progress suggests expansion. In this work move limits are denoted δ and operate collectively on all true variables such that

$$\max\left(\rho_i^{(n)} - \delta, 0.0\right) \leq \rho_i^{(n+1)} \leq \min\left(\rho_i^{(n)} + \delta, 1.0\right) \quad \forall i \tag{31}$$

and similarly for all $x_{jc}^{(n)}$, but not the artificial variables y_k^n where the initial bounds are maintained throughout to ensure LP feasibility. Rather than the objective merit function (28), we monitor the oscillation merit function (32).

$$\Phi_{\text{osc}}^{(n)} = \Phi_0^{(n)} \left(1 + \max\left(g_k^{(n)} - g_k^{\max}, 0.0\right)\right) \quad \forall k \tag{32}$$

Contrary to (28), the merit function (32) maintains a direct measure of infeasibility even for all $y_k^{(n)} = 0.0$ which is found more efficient by experience. Let $O^{(n)}$ denote the oscillation indicator for iteration (n) such that

$$O^{(n)} = \frac{\Phi_{\text{osc}}^{(n)} - \Phi_{\text{osc}}^{(n-1)}}{\Phi_{\text{osc}}^{(n-2)} - \Phi_{\text{osc}}^{(n-1)}} \tag{33}$$

Pseudo code for reduction or expansion of the move limits δ, depending on the oscillation indicator, appears in Fig. 3.

In the pseudo code shown in Fig. 3, $\alpha \in [0.0, 1.0[$ is the move limit reduction factor, $\beta \geq 1.0$ is the move limit expansion or recovery factor, and *OscCheck* prevents modification of move limits immediately upon reduction for stabilization, initialized to $OscCheck = -1$. In this work, $\alpha = 0.5$ and $\beta = 4.0$ are found appropriate.

if ($OscCheck > 0$) **then**
  if $\left(O^{(n)} < 0.0\right)$ **then**
    $\delta = \delta\alpha$
    $OscCheck = 0$
  else
    $\delta = \min\left(\delta\alpha^{-\frac{1}{\beta}}, \delta^{\text{ini}}\right)$
  end if
else
  $OscCheck = OscCheck + 1$
end if

Figure 3: Pseudo code for controlling the reduction or expansion of the move limits δ

2.5.3 Continuation strategy

Experience has shown it efficient to increase the penalization power p in a stepwise manner, known as a continuation approach. Instead of starting out from the seemingly obvious and classical case without penalization, i.e., from $p = 0.0$, it is noticed that the bi-linear product between the variables ρ_i and x_{jc} in (5) is unconditionally non-convex. An extensive parameter study has revealed it to be efficient to start out from a limited but still noticeable penalization level. The parameter study has shown the sequence

$$p = \{1.0, 2.0, 4.0\} \tag{34}$$

to be robust for all considered cases. Notice that the sequence (34) is allowed to finish prematurely in case of achieving a satisfactory feasible, near 0/1 design before the last step. This is elaborated in Section 2.5.4.

2.5.4 Convergence requirements

A continuation step is converged when fulfilling three Convergence Criteria (CC): At first, we require a sufficiently small change in the merit function (28) (CC1). This has been established to indicate if the optimization procedure has converged to a minimum. Secondly, we require vanishing artificial variables (CC2), and thirdly, we require an acceptable level of feasibility (CC3). The procedure is outlined in the following. Ultimately, fulfilment comes down to comparison with appurtenant tolerances, denoted ϵ.

A sufficiently small, absolute change in the merit function (28) is defined as

$$\left|\frac{\Phi_0^{(n)} - \Phi_0^{(n-1)}}{\Phi_0^{(n-1)}}\right| < \epsilon_\Phi \qquad \text{(CC1)} \tag{35}$$

Vanishing artificial variables are defined as

$$\left\|y_k^{(n)}\right\|_\infty < \epsilon_y \ \ \forall k \qquad \text{(CC2)} \tag{36}$$

Lastly, acceptable feasibility is defined as

$$\left\|g_k^{(n)} - g_k^{\max}\right\|_\infty < \epsilon_g \ \ \forall k \qquad \text{(CC3)} \tag{37}$$

In case of satisfactory CC's, whether or not to proceed to the next continuation step, if any, depends on the obtained level of discreteness of the design variables. To this end we introduce two slightly modified measures of non-discreteness compared to those applied in Sørensen and Lund (2013), taking into account e.g., different sizes of the sub-domains, Ω_{dl}. The measures M_{dnd} and M_{cnd} denote the density (ρ_i) and candidate (x_{jc}) non-discreteness, respectively.

$$M_{dnd}^{(n)} = \frac{4\sum_{d,l} V_{dl}\, \rho_i(1-\rho_i)}{\sum_{d,l} V_{dl}} \cdot 100\% \tag{38a}$$

$$M_{cnd}^{(n)} = \frac{\sum_{d,l} V_{dl}\, \rho_i^2 \prod_{c=1}^{n^c}\left(\frac{1-x_{jc}}{1-\frac{1}{n^c}}\right)^2}{\sum_{d,l} V_{dl}\, \rho_i} \cdot 100\% \tag{38b}$$

Most places in (38) and the following, the iteration superscript (n) is omitted for clarity. Proper association between indices dl, i, and j, as exemplified in (6), is a prerequisite for both measures. The measure of density non-discreteness M_{dnd} is normalized to yield 0.0% in case $\rho_i \in \{0, 1\}\ \forall i$ and 100.0% in case $\rho_i = 0.5\ \forall i$. The measure of candidate non-discreteness M_{cnd} is linearly dependent upon the appurtenant values of ρ_i such that it yields 100.0% for $x_{jc} = \frac{1}{n^c}\ \forall (j, c)$ if $\rho_i = 1.0\ \forall i$ and 50.0% if $\rho_i = 0.5\ \forall i$, and so on. The M_{cnd} measure yields 0.0% in case $x_{jc} \in \{0, 1\}\ \forall (j, c)$ independent of ρ_i, or in case $\rho_i = 0.0\ \forall i$ independent of x_{jc}. This linear ρ_i dependence is fair in that a distinct candidate selection is insignificant for vanishing topology variables. Continuation to the next penalization step, if any, is found relevant only in case

$$M_{nd} = \max\left(M_{dnd}^{(n)}, M_{cnd}^{(n)}\right) > \epsilon_{0/1} \tag{39}$$

Pseudo code for the convergence requirements appears in Fig. 4.

if (CC1 $< \epsilon_\Phi$) **then**
  if $\left(\text{CC2} < \epsilon_y\right)$ **then**
    if $\left(\text{CC3} < \epsilon_g\right)$ **then**
      if ($p < p_{\max}$ .and. $M_{nd} > \epsilon_{0/1}$) **then**
        Increase penalization power p
        $\delta = \delta^{\text{ini}}$
        $OscCheck = -1$
      else
        Convergence
      end if
    end if
  else
    Restart optimization
    $c = 10.0c$
  end if
end if

Figure 4: Pseudo code detailing the convergence requirements

It is seen in Fig. 4, that in case (CC1 $< \epsilon_\Phi$) but (CC2 $> \epsilon_y$), it appears that the current penalization constant c was

insufficient to ensure near zero valued artificial variables. As Svanberg (2004) suggests, c is increased, here by a factor 10.0, and the optimization problem is restarted. In case the convergence requirements on ϵ_Φ and ϵ_y are met, it comes down to the requirement on ϵ_g whether additional iterations and move limit modifications are required to facilitate final convergence. Otherwise, a new continuation step, if any, with increased penalization power p is initiated, however, only in case of an unacceptable level of non-discreteness, governed by M_{nd}. In case of continuation with increased p, the optimization problem at hand has changed for which reason move limits δ and the counter *OscCheck* are consistently relaxed to accommodate this new problem. Experience has shown that $\epsilon_\Phi = \epsilon_g = 10^{-3}$, $\epsilon_y = 10^{-4}$, and $\epsilon_{0/1} = 0.1\%$ entail an acceptable tradeoff between the required number of iterations and feasibility and discreteness of the results.

Results to follow are computed by use of our in-house finite element and optimization framework, the so-called MUltidisciplinary Synthesis Tool (MUST), see MUST (2013), which is compiled using Intel Visual Fortran together with the Intel MKL library. In order to cope with the large number of linear constraint equations stemming from the candidate material formulation (3) and the manufacturing constraints (7), (8), and (9), version 7.2-9 of the Sparse Nonlinear OPTimizer (SNOPT) by Gill et al. (2005) is applied. For all results to follow, SNOPT has been configured with default settings to solve the mathematical programming problem (30) through the presented SLP approach.

2.6 Simple 0/1 rounding

The considered optimization problem (11) is challenging to drive to *completely* binary design variables with the suggested density approach. This is primarily because of structural sensitivities of both operational signs, but likewise due to the difficult manufacturing constraints. In this work, we apply simple rounding of the design variables to finalize the obtained results into truly discrete designs, and leave for instance advanced finalization techniques, or explicit penalization of intermediate designs to future work. Let ρ_i^* denote the topology variable value after simple rounding, defined as

$$\rho_i^* = \begin{cases} 1 & \text{if} \quad \rho_i \geq 0.5 \\ 0 & \text{else} \end{cases} \tag{40}$$

Let x_{jc}^* denote the candidate variable values after simple rounding, defined such that only the originally dominating candidate c is rounded up for all candidate domains j, given as

$$x_{jc}^* = \begin{cases} 1 & \text{for} \quad \max\left\{x_{j1}\ ,\ x_{j2}\ ,\ \ldots\ ,\ x_{j(n^c)}\right\} \\ 0 & \text{else} \end{cases} \tag{41}$$

Notice that such simple rounding does not guarantee feasibility nor optimality of the posed optimization problem (11), see Nemhauser and Wolsey (1988). However, as results in Section 4 will demonstrate, obtained measures of non-discreteness M_{nd} are mostly *near-zero*, thereby indicating only minor perturbations upon rounding. The effect of the suggested simple rounding appears in Section 4 and is discussed further in Section 5.

3 Numerical examples

This section introduces several numerical optimization problems concerning a finite element model of a generic main spar used in many designs of wind turbine blades. The parameterization into candidate and geometry domains, directly associated with the design variable distribution, is however unique for all problems, i.e., Steps 1-2 are identical, but Steps 3-4 differ for all problems, see Fig. 1.

3.1 The finite element model

The geometry of the main spar is identical to the one applied in Lindgaard and Lund (2010) where fiber orientations were optimized with respect to buckling load factors applying geometric non-linear analysis. The considered main spar is truncated to a length of 14.0m and has an inner diameter of 0.88m at the fixed root section. The finite element model of the main spar appears in Fig. 5 and consists of 1,792 degenerated 9-node ESL shell elements with five DOF's per node, resulting in a total of 36,160 DOF's. See e.g., Ahmad et al. (1970) or Panda and Natarajan (1981) for element details. All ESL shell elements represent 20 layers, each with a uniform thickness. A ply thickness of 2.5mm has been selected as a tradeoff between the number of design variables and the total thickness required in order to have a realistic load case. The finite element mesh discretization of Fig. 5 has been checked for convergence as follows: Modeling the main spar entirely with 0° plies oriented along the global z-axis ($m = 2752.27$kg), the mesh was refined until stable values of the tip displacement ($u_{\text{tip}} = 0.5846$m) and the lowest buckling load factor ($\lambda_1^{(b)} = 8.810$) and eigenfrequency ($\omega_1 = 4.378 \cdot 2\pi \frac{\text{rad}}{\text{s}}$) were obtained. The main spar is modeled with clamped boundary conditions at the circular end of the root section and the applied tip load resembles the most critical load case for the wind turbine blade, a so-called 50 year gust scenario, subjecting the blade to a case of extreme flap-wise bending. The load is introduced as a uniform pressure, illustrated by the hatched rectangle at the tip in Fig. 5. The distributed load has an intensity of

$$q = \frac{164.7\text{kN}}{0.3\text{m} \cdot 1\text{m}} = 559\text{kPa} \tag{42}$$

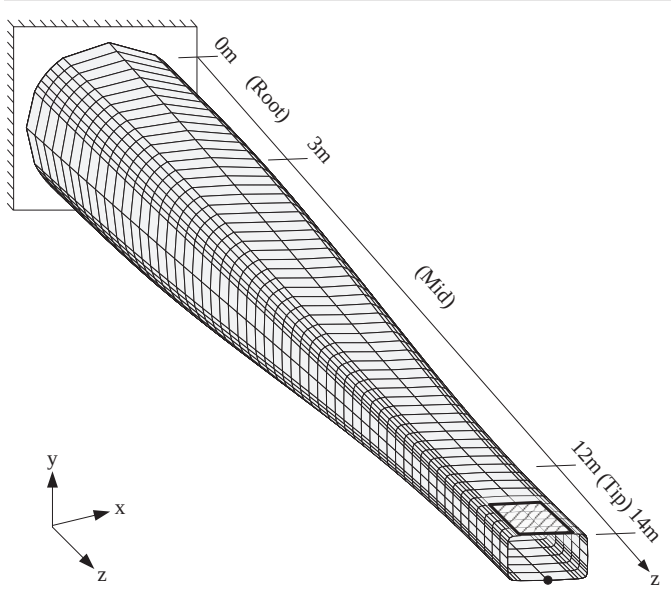

Figure 5: Finite element model of a generic main spar, clamped at the circular end of the root section and tapered towards the tip that is subjected to a uniform pressure load at the hatched rectangular area. Cross sections of the root and the tip appear in Fig. 6. All ESL shell elements have their first principal material direction aligned with the global z-axis, and their surface normals pointing outwards. At the tip, the node marked by the bottom dot is subjected to a displacement constraint

The structural setup resembles testing of wind turbine blades in a controlled environment, see Overgaard et al. (2010). Neither the geometry of the main spar nor the applied load case introduce torsion into the model. Geometric linear analysis is used throughout this paper to limit the computational time. The proposed method does, however, allow for the use of geometric non-linear analysis, and the authors recognize the limitations associated with linear analyses. This is further discussed in Section 5.1. Lindgaard and Lund (2010) showed that geometric linear analysis generally overestimates the critical load in buckling load optimization.

3.2 Parameterization of the generic main spar

Parameterization of the finite element model is an important step in the optimization procedure as structural performance and manufacturability of the optimized designs depend hereupon. The production method for the presented main spar relies on the application of a mandrel that essentially dictates the inner shape of the main spar. The root of the mandrel is bolted to a rigid wall and the mandrel is then covered by mats or blocks of different materials and principally "built up" from the inside in a series of steps. First, GFRP biax fiber mats are typically wrapped around the full length of the mandrel. Next, full-length GFRP UD fiber mats are rolled along the top and bottom surfaces of the mandrel. On the sides/webs of

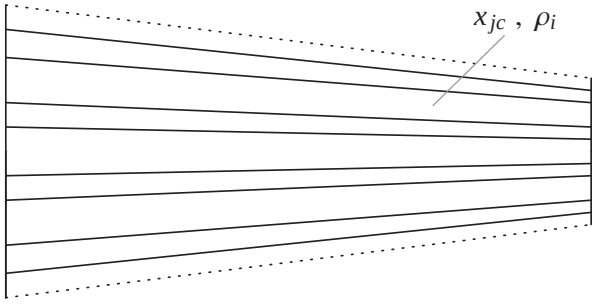

Figure 7: The longitudinally coinciding candidate and geometry domain parameterization is referred to as the Long-Long parameterization

the mandrel, blocks of lightweight foam or balsa material are positioned. These steps are systematically repeated, resulting in a structure with varying thickness at different locations around the mandrel. Finally, the composite structure is cured and the finished main spar can be pulled off the mandrel. With this production method in mind, an obvious question crops up, namely where to most appropriately allocate the available material candidates, to obtain a high-performance, manufacturable structure? The design freedom, but hence also the potential level of structural complexity, is directly linked to the parameterization into geometry and candidate domains, see Fig. 1. If, for instance, the manufacturer is accustomed to apply large rolls of fibrous material with a width of 1.0m, then the parameterization into geometry and candidate domains should accommodate just this. In this work, we compare the optimization outcomes on basis of nine representative candidate and geometry parameterizations of the generic main spar. This is done to give insight into the relation between potential weight saving and complexity, subject to identical structural criteria and manufacturing constraints. The constraint specifications are elaborated in Section 3.2.2.

The finite element mesh discretization of Fig. 5 (Step 1 in Fig. 1) is deemed too fine for the arrangement into sub-domains Ω_{dl} (Step 2 in Fig. 1). The arrangement of the main spar mesh into sub-domains appears in Fig. 6 that illustrates the main spar, cut along the longitudinal direction of the upper surface (the dotted lines) and unfolded as a flat surface. The main spar mesh is arranged into a total of $28 \times 8 = 224$ sub-domains, identical for all layers. The sub-domains are equally spaced longitudinally. Circumferentially, the sub-domains vary in width, see the bold line markings to the left and right of Fig. 6. Concerning Steps 3-4 in Fig. 1, i.e., the parameterization into geometry domains and candidate domains, associated with variables x_{jc} and ρ_i, respectively, the following nine parameterizations are considered. The nine parameterizations are constructed on basis of Fig. 7 and Fig. 8, where the sub-domains are parameterized into coinciding candidate and geometry domains longitudinally and circumferentially, respectively. Figure 7 represents

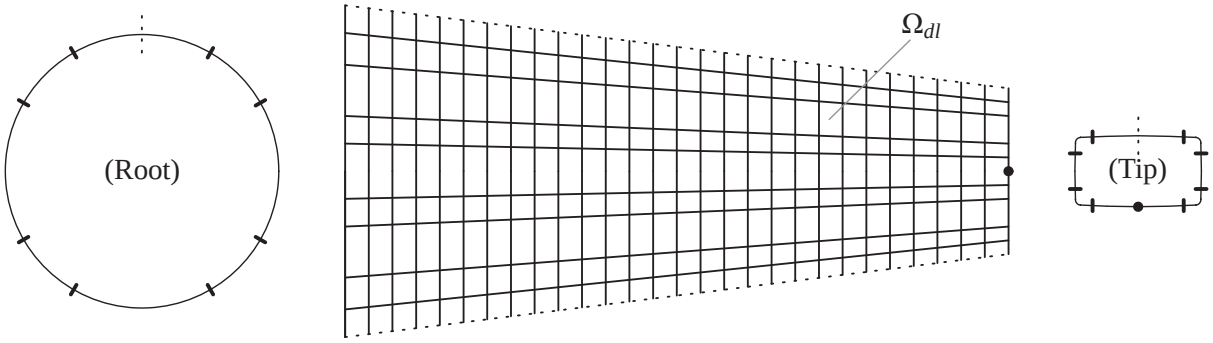

Figure 6: *Left:* Cross sectional view of the circular root section. Bold lines denote eight circumferential design domain arrangements. *Mid:* Unfolded surface view of the main spar, cut along the longitudinal direction of the upper surface. The cut is illustrated by the dotted lines. The generic main spar mesh is arranged into $28 \times 8 = 224$ sub-domains, Ω_{dl}. *Right:* Cross sectional view of the tip section

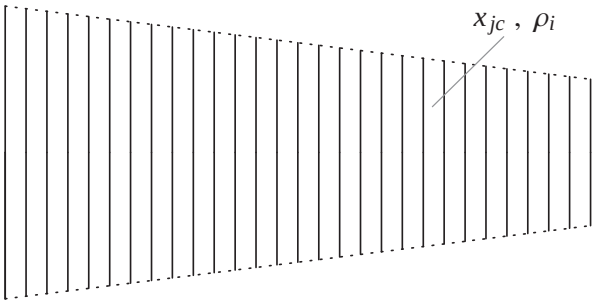

Figure 8: The circumferentially coinciding candidate and geometry domain parameterization is referred to as the Circ-Circ parameterization

a parameterization where both the candidate domains x_{jc} *and* the geometry domains ρ_i coincide longitudinally. For this reason we denote this parameterization Long-Long for candidate domains, x_{jc}, and geometry domains, ρ_i, respectively. Similarly, Fig. 8 represents the so-called Circ-Circ parameterization with circumferentially coinciding candidate domains, x_{jc}, and geometry domains, ρ_i, respectively. These particular parameterizations represent a relatively low level of complexity, i.e., a high degree of manufacturability. For this reason, exactly these two parameterizations are considered in detail in the following sections. The low level of complexity associated with these particular parameterizations is in contrast to the so-called Grid-Grid parameterization, where candidate and geometry domains coincide with the sub-domain arrangement in Fig. 6. This parameterization is hence considered quite complex and difficult to manufacture. Allowing candidate and geometry domains to be non-coinciding within the three described parameterization types, i.e., the longitudinal (Long), the circumferential (Circ), and the grid type (Grid) parameterizations, a total of nine uniquely defined candidate-geometry domain parameterizations can be defined, see Table 1. These nine parameterizations into candidate domains, x_{jc}, and geometry domains, ρ_i, give insight into the relation between potential weight saving and complexity.

Table 1: The nine considered parameterizations into candidate domains, x_{jc}, and geometry domains, ρ_i

Candidate domains (x_{jc})		Geometry domains (ρ_i)
Long	-	Long
Long	-	Circ
Long	-	Grid
Circ	-	Long
Circ	-	Circ
Circ	-	Grid
Grid	-	Long
Grid	-	Circ
Grid	-	Grid

Table 2: Properties of the considered candidates

Property	Units	UD	Biax	Foam
E_{11}	[GPa]	34.00	16.50	0.16
E_{22}	[GPa]	8.20	16.50	-
E_{33}	[GPa]	8.20	8.20	-
G_{12}	[GPa]	4.50	9.50	-
G_{23}	[GPa]	4.00	4.00	-
G_{13}	[GPa]	4.50	4.50	-
ν_{12}	-	0.29	0.29	0.45
ϱ	[kg/m^3]	1910.00	1910.00	130.00

3.2.1 Candidate materials

The numerical examples include six different candidate materials commonly applied in the wind turbine industry, i.e., $n^c = 6$. Candidates one to four represent GFRP UD plies with $\{-45°, 0°, 45°, 90°\}$ fiber orientations. The 5th candidate represents a GRFP $\{\pm 45°\}$ biax ply with properties obtained on basis of the $\{-45°, 45°\}$ UD data. The 6th and last candidate represents a lightweight isotropic foam material such that a sandwich structure is a possible outcome of the optimization problem. Candidate properties appear in Table 2. The void material, $\boldsymbol{E}_0$ from (5),

Table 3: Settings concerning structural criteria and manufacturing constraints

$\underline{\lambda}^{(b)}$	$\underline{\omega} = \sqrt{\underline{\lambda}^{(f)}}$	$\overline{u}$	$n_\lambda^{(b)}$	$n_\lambda^{(f)}$	S	CL	T
3.0	$2\pi\frac{\text{rad}}{\text{s}}$	1.0m	10	10	2	8	0.10

is modeled as a weightless isotropic material with one millionth the stiffness of the GFRP UD candidate, i.e., $E_{11} = 34$kPa, and identical Poisson's ratio. Because other industries do not allow sandwich designs, results for the nine parameterizations in Table 1 will also be listed without foam as a candidate, in which case $n^c = 5$. Consequently, the considered number of design variables varies between 953 for the Long-Long parameterization without foam to 31,137 for the Grid-Grid parameterization including foam. Notice that for all parameterizations, the entire innermost layer of the generic main spar is modeled as a single, unity valued topology variable to eliminate the risk of holes through the thickness.

3.2.2 Constraint specifications and initial settings

In agreement with the main spar study in Overgaard et al. (2010), the representative bounds listed in Table 3 have been chosen for the structural constraints in (11b)-(11d). In order to cope with potentially shifting eigenvalues, we consider the first ten buckling load factors and eigenfrequencies, assumed ordered by magnitude. The displacement constraint limits the global y-displacement of the bottom tip node, marked in Fig. 5, preventing collision between blade and tower. With respect to the manufacturing constraints (11e), see Section 2.3 for details, we apply the limit values apparent rightmost in Table 3. A thickness variation rate of ± 2 plies ($S = 2$) between adjacent geometry domains, ρ_i, is used to ensure sufficiently smooth external ply drop transitions for all parameterizations of the generic main spar. For the particular main spar example considered in this work, we apply a contiguity limit as large as eight identical plies through the thickness ($CL = 8$), being considerably more than the commonly applied limit of four, see e.g., Le Riche and Haftka (1993) or Toropov et al. (2005). Nevertheless, the wind turbine industry is less restrictive than the aerospace industry; hence larger amounts of identical UD plies can be accepted. The influence of the applied contiguity limit is further scrutinized in the discussion of the results. These settings imply that the number of MC's vary between 1,144 for the Long-Long parameterization without foam to 20,800 for the Grid-Grid parameterization including foam with 21,584 and 182,016 non-zero coefficient matrix entries, respectively. The design variables are initialized as $x_{jc} = \frac{1}{n^c}$ for all candidate variables and $\rho_i = 1.0$ for all topology variables to start out as feasible as possible without candidate preference, found efficient by experience. This implies an initial mass $m = 2324.78$kg or $m = \overline{m} = 2752.27$kg, including or excluding foam as a candidate, respectively, where $\overline{m}$ denotes the maximum attainable mass. The potential to obtain a feasible solution with an end mass lower than $\overline{m}$ is clear from a comparison with the presented values from modeling the main spar entirely with 0° plies oriented along the global z-axis, see Section 3.1. Move limits are initialized as $\delta^{\text{ini}} = 0.20$. The move limit range $0.0 \leq \delta \leq \delta^{\text{ini}}$ is adaptively modified as prescribed in Section 2.5.

4 Results

Tables 4-5 provide detailed result overviews of the DMTO approach of the nine different parameterizations introduced in Section 3, both with and without foam as a candidate. Table 4 presents the original, non-rounded results on basis of the SLP approach presented in Section 2.5. A star $*$ in front of the total number of iterations $\#It$. indicates that the SLP approach has been restarted once with up-scaled c value to obtain vanishing artificial variables, y_k. Table 5 presents the results upon finalization by the simple rounding described in Section 2.6. The results in Table 4 and Table 5 are referred to as original and rounded results, respectively. For easy comparison, Fig. 9 provides a graphical overview of the original DMTO results of the nine parameterizations with foam. In the figure, measures of non-discreteness, M_{nd} from (39), above 1.0% have been truncated. See Table 4 for details. As mentioned previously in Section 3.2, rounded results of the Long-Long and Circ-Circ parameterizations with and without foam, respectively, are picked out for detailed representations given their limited complexity. Apart from demonstrating the versatility and robustness of the DMTO method, results from the additional parameterizations primarily serve a comparative purpose in order to assess the relation between potential weight saving and complexity for the considered main spar example. Figure 10 illustrates an exploded view of the allocation of candidates for the Long-Long parameterization with foam, seen from the fixed root end. Candidate allocation is identical longitudinally. Notice that the allocation among the candidates depicted to the right of Fig. 10 is given with respect to a local coordinate axis, denoted y'. Figure 11 illustrates the allocation of candidates for the Circ-Circ parameterization without foam where bottom and top illustrate the inner and outer surfaces, respectively. Candidate allocation is identical circumferentially. Figure 12 shows the design iteration history for the Long-Long parameterization with foam, illustrating the evolution of m, $\lambda_1^{(b)}$, $\lambda_1^{(f)}$, $|u_o|$, M_{cnd}, M_{dnd}, $\|y_k\|_\infty$, $\|g_k - g_k^{\max}\|_\infty$, and $\Delta(x_{jc}, \rho_i)$; see the caption for further explanations and normalization details.

Table 4: Tabular overview of the original DMTO results of all parameterizations, both with and without foam as a candidate. $\#It.$ denotes the total number of iterations. A star $*$ in front of $\#It.$ denotes that the SLP approach has been restarted once with up-scaled c value

Parameterization	With foam						Without foam					
$(x_{jc} - \rho_i)$	m [kg]	$\frac{\lambda_1^{(b)}}{\underline{\lambda}^{(b)}}$	$\frac{\lambda_1^{(f)}}{\underline{\lambda}^{(f)}}$	$\frac{\lvert u\rvert}{\overline{u}}$	M_{cnd}/M_{dnd} [%]	$\#It.$	m [kg]	$\frac{\lambda_1^{(b)}}{\underline{\lambda}^{(b)}}$	$\frac{\lambda_1^{(f)}}{\underline{\lambda}^{(f)}}$	$\frac{\lvert u\rvert}{\overline{u}}$	M_{cnd}/M_{dnd} [%]	$\#It.$
Long-Long	1249	1.000	2.969	1.000	0.282 / 0.672	41	1802	1.000	4.218	1.000	0.000 / 3.079	49
Long-Circ	1240	1.037	2.938	1.000	0.062 / 0.000	28	1841	1.081	4.328	0.999	0.001 / 0.451	44
Long-Grid	1225	1.000	2.926	1.000	0.159 / 0.999	40	1807	1.118	4.378	1.000	0.000 / 1.728	*142
Circ-Long	1431	0.999	5.008	1.000	0.180 / 0.000	41	1850	1.117	4.178	1.000	0.815 / 0.273	39
Circ-Circ	1519	1.001	4.690	0.999	0.316 / 0.305	*91	1854	1.069	4.334	1.001	0.829 / 0.971	44
Circ-Grid	1428	1.000	5.019	1.000	0.139 / 1.518	57	1746	1.014	4.466	1.000	0.559 / 2.177	54
Grid-Long	1171	0.999	2.738	1.000	0.671 / 0.120	63	1818	1.148	4.205	0.999	3.517 / 0.984	48
Grid-Circ	1181	0.999	2.787	1.000	0.947 / 0.196	84	1848	1.095	4.252	1.001	2.715 / 0.337	44
Grid-Grid	1163	0.999	2.789	1.000	1.053 / 1.408	81	1734	1.000	4.455	1.000	1.619 / 1.446	64

Table 5: Tabular overview of the rounded DMTO results of all parameterizations, both with and without foam as a candidate

Parameterization	With foam					Without foam				
$(x_{jc} - \rho_i)$	m [kg]	$\frac{\lambda_1^{(b)}}{\underline{\lambda}^{(b)}}$	$\frac{\lambda_1^{(f)}}{\underline{\lambda}^{(f)}}$	$\frac{\lvert u\rvert}{\overline{u}}$	# Violated MC's	m [kg]	$\frac{\lambda_1^{(b)}}{\underline{\lambda}^{(b)}}$	$\frac{\lambda_1^{(f)}}{\underline{\lambda}^{(f)}}$	$\frac{\lvert u\rvert}{\overline{u}}$	# Violated MC's
Long-Long	1246	0.930	2.961	0.995	0	1832	1.138	4.282	0.953	0
Long-Circ	1242	1.081	2.951	0.999	0	1837	1.081	4.358	0.998	0
Long-Grid	1221	0.970	2.950	1.001	0	1805	1.143	4.396	0.994	0
Circ-Long	1431	0.964	5.006	0.999	0	1848	1.121	4.180	1.001	0
Circ-Circ	1520	0.970	4.656	0.994	0	1844	1.069	4.378	1.003	0
Circ-Grid	1429	0.935	5.054	0.994	0	1734	1.017	4.477	1.003	0
Grid-Long	1159	0.887	2.738	1.001	0	1832	1.185	4.249	0.967	29
Grid-Circ	1159	0.873	2.804	1.004	0	1846	1.101	4.280	0.994	41
Grid-Grid	1140	0.807	2.776	1.002	0	1733	1.028	4.478	0.995	0

5 Discussion

The discussion of the results is done in the following steps. Initially, some general comments about the original non-rounded results are stated. Secondly, the overall effects of rounding are discussed. Thirdly, we discuss the results of the Long-Long and Circ-Circ parameterizations, respectively, with and without foam in detail. Finally, general comments about the performance of the DMTO method are stated.

5.1 Original result tendencies

It is clear from the results of Table 4 and Fig. 9 that parameterizations with foam as a candidate significantly outperform those without foam. The optimizer recognizes the foam candidate as a profitable means of obtaining high moments of inertia, beneficial for the considered flap-wise bending load case. With foam, the end mass ranges from $0.42\overline{m} \leq m \leq 0.55\overline{m}$ as opposed to a range from $0.63\overline{m} \leq m \leq 0.67\overline{m}$ without foam. The lowest mass is 1163kg for the original Grid-Grid parameterization with foam, and the largest being 1854kg for the original Circ-Circ parameterization without foam. It is not surprising that the Grid-Grid parameterization with foam yields the lowest mass as this parameterization reflects ultimate design freedom, supporting rapid changes in both geometry and candidate preference. Hence, the Grid-Grid result with foam should be the natural choice for a high-performance design; that is *if* manufacture is possible, which is doubtful due to the high degree of complexity. The displacement constraint is active for all parameterizations. Most parameterizations do likewise end up with active constraints on buckling load factors, whereas the constraints on eigenfrequencies are inactive throughout as a consequence of low mass and high stiffness. Neverthe-

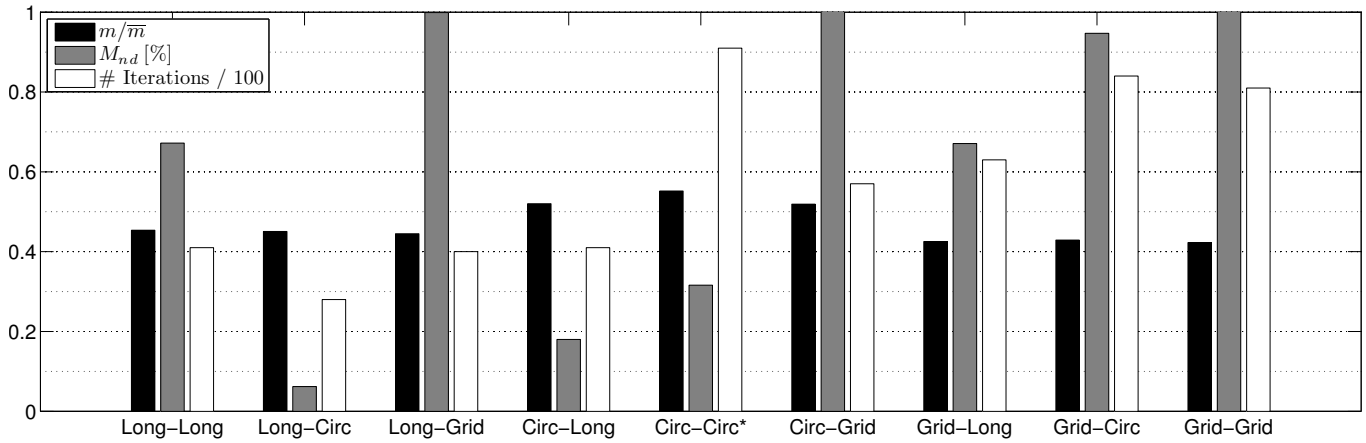

Figure 9: Graphical result overview of the original DMTO results of the 9 parameterizations with foam. The star marking at Circ-Circ* denotes that the SLP approach has been restarted once with up-scaled c value. M_{nd} measures are truncated at 1.0%, see Table 4 for details

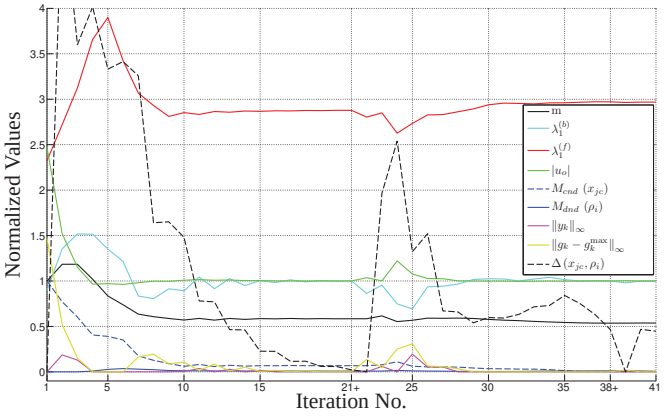

Figure 12: Design iteration history for the Long-Long parameterization with foam. The mass m is normalized with respect to the initial mass. The structural performance constraints $\lambda_1^{(b)}$, $\lambda_1^{(f)}$, and $|u_o|$ are normalized with respect to their bounds, see Table 3. The measures of non-discreteness, M_{cnd} and M_{dnd}, appear as decimal numbers. The values of the largest artificial variable, $\|y_k\|_\infty$, and the largest infeasibility among the structural constraints, $\|g_k - g_k^{\max}\|_\infty$, are shown in accordance with (36) and (37), respectfully. $\Delta(x_{jc}, \rho_i)$ is the Euclidean norm of the change in design variables between two successive iterations. A change in penalization is indicated with a "+" sign next to the iteration number in which the penalization was increased

less, one can only ensure demands on structural criteria when present in the optimization problem.

As highlighted in Section 3.1, the numerical examples have been conducted using geometric linear finite element analysis. In order to estimate the effects of the geometric non-linearity on the active constraints, a geometric non-linear analysis of the two initial designs for the parameterizations with and without foam as a material candidate, see Section 3.2.2, has been conducted. These analyses show that the linear tip displacement is within 5% of the geometric non-linear tip displacement. The buckling analysis comparison revealed that the linear predictions are up to 17% larger for parameterizations without foam, and 10% larger for parameterizations with foam. In spite of these deviations, we maintain linear analyses to reduce the computational time. It is, however, stressed that the DMTO method supports non-linear analyses as well.

In section 2.4, we state that including $n_\lambda^{(b)}$ buckling load factors takes care of crossing eigenvalues (mode switching) during the optimization process. In all the numerical examples, the ten lowest buckling load factors were thus included as constraints in the optimization problem. To check if including the ten lowest values has sufficed, the final ten buckling load factors have been analyzed for all numerical examples. Here it has been found that the difference in magnitude between the first and the 10th value is on average 17% and 28% for the parameterizations with and without foam, respectively. The possibility for the 11th load factor changing more than 17% or 28% between two successive iterations is believed to be negligible; hence including the ten lowest positive buckling load factors has been adequate for controlling mode switching for the applied numerical examples.

The measures of non-discreteness, M_{cnd} and M_{dnd} from (38), are generally largest for the Grid-Long, Grid-Circ, and the Grid-Grid parameterizations without foam. The reason for this may be that this particular group of parameterizations represents the most challenging optimization problems, considering the number of design variables, the number of constraints, and the fact that those parameterizations without foam call for a larger extent of thickness variation than parameterizations with foam where sandwich structures are natural outcomes. Experience has shown that neither increasing penalization nor different continuation approaches improve the obtained levels of non-discreteness. One way of addressing this issue could be to use explicit penalization of intermediate valued design variables as suggested in e.g., Hvejsel et al. (2011) or Kennedy and Martins (2013). Modification or even re-

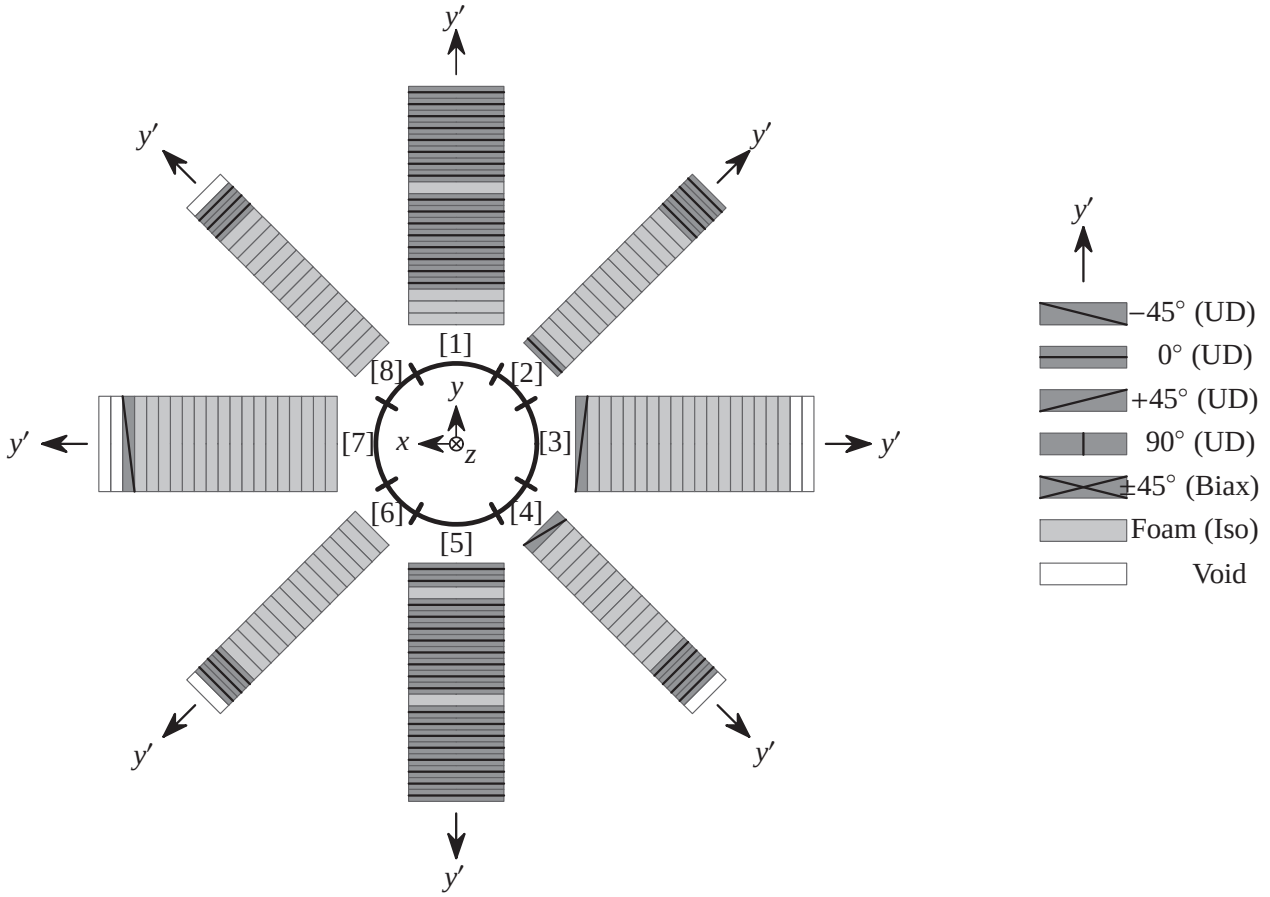

Figure 10: Rounded DMTO result of the Long-Long parameterization with foam. The Long-Long parameterization implies that candidate allocations and thicknesses of the eight longitudinal design domains, marked by [1]-[8], are identical from the root to the tip of the main spar

moval of the troublesome constraints that prevent intermediate void (MC4), see (9), is likewise considered attractive as it may facilitate application of highly robust SQP or interior point optimizers, see Sørensen and Lund (2013) for further discussion on this issue. The obtained levels of non-discreteness are all less than 4% which is found acceptable. Robust solutions for obtaining even more discrete results at this stage, i.e., prior to the following finalization by rounding, are left for future work. Notice that the Long-Circ parameterization with foam converges before the last continuation step as a result of a sufficiently near-zero measure of non-discreteness, M_{nd}, see (39).

The total number of iterations ranges from 28-142 with an average of 59. The star $*$ in front of the two parameterizations in Table 4; Circ-Circ and Long-Grid, with and without foam, respectively, denotes that these particular parameterizations were restarted once with up-scaled c values to obtain vanishing artificial variables, y_k. Experience has shown that the initial value $c = 100.0$ yields better results than $c = 1000.0$ or more for which reason up-scaling is only applied if necessary in agreement with Svanberg (2004).

The sequential time consumption associated with DSA exceeds the evaluation of structural criteria by a factor of 18 to 22. The DSA time of the Grid-Grid parameterization with foam exceeds that of the Long-Long parameterization with foam by 22%. Given that these two parameterizations involve 31,137 and 953 design variables, respectively, clearly demonstrates the efficiency of the adjoint formulation when having many design variables.

The three-step continuation sequence (34) is found to yield better results than applying a single, constant penalization value throughout. Likewise, the sequence is found more robust than additional continuation steps or even starting out from lower values of p. Too many continuation steps impose a risk of getting stuck at an intermediate design point with no chance of getting rid of the artificial design variables.

5.2 Rounded result tendencies

Results upon finalization by the simple rounding described in Section 2.6 appear in Table 5. The effect of rounding on the original mass varies between -23kg for the Grid-Grid parameterization with foam to +30kg for the Long-Long parameterization without foam. Changes in the original mass are generally reflected upon changes in the criteria functions. Rounding generally affects the parameterizations with foam as a candidate significantly more than those without. This is due to the large differ-

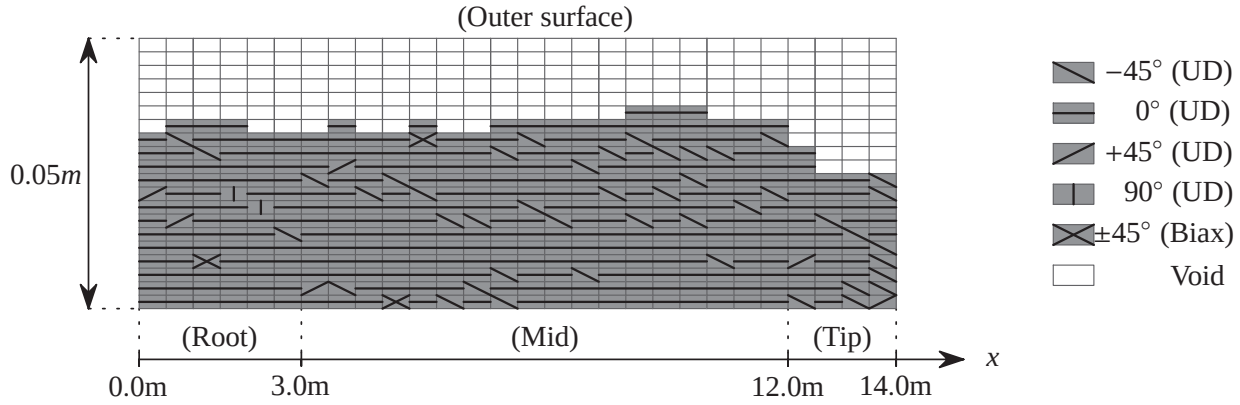

Figure 11: Rounded DMTO result of the Circ-Circ parameterization without foam. The Circ-Circ parameterization implies that the candidates are distributed in 0.5m wide circular belts, wrapped around the entire circumference of the main spar, resulting in 28 unique candidate belts throughout the length

ence in the constitutive properties, see Table 2. The buckling criterion is particularly affected, being more locally dependent upon change than e.g., the tip displacement constraint. Rounding of the Grid-Grid parameterization with foam yields a buckling load factor constraint violation of 19.3%. On average, however, rounding causes structural criteria constraint perturbations < 3%.

Rounding of the two parameterizations; Grid-Long and Grid-Grid, both without foam, causes 29 and 41 violations of the manufacturing constraints, respectively. The violations are in both cases associated solely with the constraints on contiguity (MC3), see Section 2.3.3, allowing at most 8 identical contiguous candidates throughout the 20 layers of the 224 candidate domains. Upon rounding, more than 8 GFRP UD plies oriented at 0° appear contiguously. As previously mentioned, infeasible constraints are a possible risk associated with this simple rounding scheme due to the decoupling of the optimizer. Nevertheless, it is stressed once more that DMTO results should not be viewed as final designs, ready to manufacture, but rather as a vital source of inspiration for thickness variation and stacking sequences throughout the entire structure.

5.2.1 Long-Long with foam

The rounded DMTO result of the Long-Long parameterization with foam appears in Fig. 10. Candidate allocation and domain thicknesses are inherently identical longitudinally, hence not allowing a tapered geometry towards the tip. Despite these inherent restrictions, the allocation of candidates agrees quite nicely with existing designs. The moment of inertia I_{xx} is large in order to cope with the displacement constrained, flap-wise bending load case. This is clear from the predominant stacking of 0° GFRP UD plies at the top and bottom domains, denoted by numbers [1] and [5] in Fig. 10, respectively. 0° GFRP UD plies likewise appear at the outermost active layers around [2], [4], [6], and [8]. These plies contribute to I_{xx} as well. The two sides [3] and [7] are free from material at the outermost two layers and otherwise predominantly constituted by the lightweight foam candidate. The bottom domain [5] contains more 0° GFRP UD plies than the top domain [1], probably to resist the first buckling loads, dominant along the bottom pressure side [5]. Notice the presence of at most eight contiguous UD plies, thereby satisfying the imposed contiguity limit (MC3). In spite of feasibility, it is, however, recognized that having too thick regions with identical fiber orientation is typically unwanted; especially in the more conservative aerospace industry. Tightening the contiguity limit to the commonly applied value of four has been tested to result in additional foam plies in between the thick stacks of 0° GFRP UD plies. Not surprisingly, a tighter contiguity limit increases the final mass.

From a manufacturing point of view, rapid encapsulation of just a few plies of foam in between fibrous layers such as occurring in [5], is undesirable. Multiple encapsulations are nevertheless a perfectly feasible outcome with the current DMTO formulation, and future work should impose the aforementioned sandwich constraints, forcing foam plies to be grouped together through the thickness of the candidate domains. Such constraints should likewise ensure the block of foam to be enclosed by fibrous material from both sides, unlike the regions [3] and [4]. Manufacturing constraints ensuring minimum proportions or presence of all material candidates as well as constraints limiting the change in fiber orientation between adjacent in-plane candidate domains could likewise be considered, but are, however, left for future extensions of the DMTO method.

Notice that the design is not entirely symmetric along the *xz* and *yz* coordinate planes. This not entirely symmetric design across the vertical *yz* plane may be a beneficial way to exploit elastic couplings, obscure at first glance. Another explanation may be that the optimizer has settled on a sub-optimal minimum. Furthermore, due to the flap-wise bending load case, the solution does not con-

tain more than three GFRP plies with other orientations than 0° in total. Had the examples been formulated with an additional torsion load case, other fiber orientations would probably occur in greater numbers. Nevertheless, the rounded result appears to provide a sound offset for detailed post-processing.

Figure 12 shows a typical iteration history graph; here for the Long-Long parameterization with foam. At the initial design point, the displacement constraint is infeasible, and the optimizer initially focuses on obtaining a feasible design at the expense of an increase in mass. Feasibility is obtained in iteration number four; showing that the merit function approach effectively copes with infeasibilities. The candidate non-discreteness is rapidly decreasing in pace with the optimizer recognizing that UD material should be allocated on the top and bottom faces of the main spar to achieve feasibility. The measure of density non-discreteness reaches its maximum value of 3.6% in the 6th iteration and drops to a stable value around 1% at the 12th iteration. At the 7th iteration, the buckling constraint becomes infeasible and remains so until iteration number 11. However, it oscillates around the feasibility limit until it becomes active at iteration number 21 which then satisfies convergence criteria CC3, causing an increase in penalization. Notice that during this phase, the change in the design variables decreases for each iteration; showing that the move-limit strategy indeed responds to oscillating constraints. Up until the first increase in penalization, the mass has decreased by 41.6% with respect to the initial mass. After this change in penalization both the displacement and buckling constraints become infeasible until activity is obtained in iteration number 29. From this iteration until the next increase in penalization, the candidate non-discreteness decreases from 5.2% to 0.26%, and the mass decreases as well until CC1 is finally satisfied. From iteration 38 to 41, the mass is increased from 1247kg to 1249kg. However, the measure of density non-discreteness is reduced from 1.1% to 0.67%. Final convergence is facilitated by satisfying CC2 and CC3 in iteration number 40 followed by CC1 in 41. Overall, the presented iteration history demonstrates that the SLP approach with merit functions is quite efficient at obtaining a feasible and near discrete design in spite of great non-linearity of the involved structural criteria.

5.2.2 Circ-Circ without foam

The rounded DMTO result of the Circ-Circ parameterization without foam as a candidate appears in Fig. 11. Generally, the combination of the flap-wise bending load case together with the displacement constraint calls for a high moment of inertia I_{xx} and hence predominantly 0° GFRP UD plies on the top and bottom faces. This is also clear from the results of the Long-Long parameterization. For the Circ-Circ parameterization the candidate domains are grouped together in circular belts around the circumference of the main spar. Consequently, the optimizer is forced to allocate the 0° GFRP UD candidate on the webs of the structure in order to also place them on the desirable top and bottom faces. The consequence of this is particularly pronounced for the parameterization with foam as a candidate material. In this case, the optimizer cannot allocate the same amount of foam on the webs as in the case of the Long-Long parameterization; ultimately resulting in a substantial increase of the final mass. Naturally surpassed by the 0° GFRP UD candidate, the −45° GFRP UD candidate is the second most present candidate. This candidate may very well represent beneficial properties to constrain the risk of buckling. The −45° GFRP UD candidate occurs in particular at the tip section where the pressure load is introduced, hence making this area prone to local buckling. The thickness is smallest at the tip section and largest between the tip and the mid-section as this region is vulnerable to buckling along the pressure side as well. Notice that the thickness is changed with at most two ply thicknesses between neighboring geometry domains, satisfying the constraints on thickness variation rate (MC2), see (7).

5.3 General performance of the DMTO approach

The capabilities of the suggested DMTO approach have been demonstrated on differently parameterized numerical examples of a main spar. The suggested SLP approach is found robust, providing near-discrete designs in an acceptable number of iterations. Simple rounding finalizes the designs, causing average structural criteria constraint perturbations < 3%, which is deemed acceptable. However, for the Grid-Long and Grid-Circ parameterizations with foam, rounding causes infeasible manufacturing constraints on contiguity.

The considered parameterizations with and without foam as a candidate do indeed give an insight into the relation between weight saving and design complexity. In the considered load case, foam is consistently an advantageous candidate. The lightest design, weighing 1163kg prior to rounding, occurred on basis of the quite complex Grid-Grid parameterization with foam, difficult if not impossible to realize with today's manufacturing techniques. In contrast, the simple Circ-Circ parameterization with foam proved inadequate for the considered load case, weighing 30.6% more than the Grid-Grid parameterization. Nevertheless, the least complex result with foam of all, being the Long-Long parameterization, ended up weighing 1250kg prior to rounding, i.e., merely 7.5% more than the complex Grid-Grid parameterization. The relation between weight saving and complexity is hence not straightforward. Complex parameterizations with great design freedom result in the largest weight savings, but are hardly manufacturable. However, fairly simple, but well-parameterized, designs may likewise per-

form well. The results in general appear to provide great inspiration for detailed post-processing. This is the exact intention of the suggested DMTO method.

6 Conclusion

In this work, we have presented a gradient based topology optimization method for minimizing the mass of large-scale laminated composite structures. The method is labelled DMTO for Discrete Material and Thickness Optimization. The DMTO method enables minimum mass designs by simultaneously determining an optimum material distribution and thickness variation. This is done while also considering industrially relevant constraints on structural performance i.e., buckling load factors, eigenfrequencies, and limited displacements. Furthermore, common design guidelines or rules, referred to as manufacturing constraints, are included explicitly as series of linear inequalities.

The capabilities of the method have been demonstrated on a generic main spar used in many designs of wind turbine blades. In order to give insight into the relation between potential weight saving and design complexity, the main spar was parameterized in different ways ranging from simple to complex to manufacture with today's production techniques in mind. The results show that some parameterizations can indeed obtain significant weight savings while also being simple to manufacture. It is thus stressed that the initial parameterization is of great importance as both the performance and the manufacturability depend hereupon.

The design of the main spar together with the applied flap-wise bending load case makes foam material an attractive candidate. The results showed that, on average, examples with foam as a candidate obtained a final mass, nearly 30% lower than those without foam as a candidate.

The preceding work by Sørensen and Lund (2013) suggests that SLP methods are favorable compared to e.g., SQP formulations. This is mainly due to the nature of the manufacturing constraint for preventing intermediate void through the thickness of the laminate. Compared to the preceding work, we are now dealing with a far more difficult problem given structural performance constraints with sensitivities of both operational signs. An SLP merit function approach, based on Svanberg (2004), was applied to pose unconditionally feasible LP problems. The SLP approach was found robust and effective, emphasized by the fact that all of the numerical examples converged to feasible designs within 28-142 iterations.

A three-step continuation approach with increasing penalization in a product of RAMP interpolation schemes was found efficient for obtaining near-discrete designs. Strictly binary designs were obtained through finalization by simple rounding, resulting in constraint perturbations $< 3\%$ in most cases. In general, the DMTO method is found as a great source of inspiration for manufacturable thickness variation and stacking sequences throughout the structure; inspiration for detailed post-processing that may very well outperform intuition, exploiting elastic couplings that may appear obscure at first glance.

Acknowledgements

This work was supported by the Danish Centre for Composite Structures and Materials for Wind Turbines (DCCSM), grant no. 09-067212 from the Danish Strategic Research Council (DSF), and by the Danish Research Council for Technology and Production Sciences (FTP), grant no. 10-082695. This support is gratefully acknowledged. The authors thank Mathias Stolpe, Technical University of Denmark, Department of Wind Energy, for fruitful discussions and inputs for this research. The final publication is available at Springer via http://dx.doi.org/10.1007/s00158-014-1047-5

References

Ahmad, S., Irons, B. M., and Zienkiewicz, O. C. Analysis of thick and thin shell structures by curved elements. *International Journal for Numerical Methods in Engineering*, 2:419–451, 1970.

Arora, J. S. *Introduction to Optimum Design*. Elsevier Academic Press, 2 edition, 2004. ISBN 0120641550.

Arora, J. and Wang, Q. Review of formulations for structural and mechanical system optimization. *Structural and Multidisciplinary Optimization*, 30(4):251–272, 2005. ISSN 1615-147X.

Bendsøe, M. P. Optimal shape design as a material distribution problem. *Structural and Multidisciplinary Optimization*, 1(4):193–202, 1989.

Bendsøe, M. P. and Sigmund, O. *Topology Optimization*. Springer Verlag, second edition, 2003. ISBN 3-540-42992-1.

Bruggi, M. and Duysinx, P. Topology optimization for minimum weight with compliance and stress constraints. *Structural and Multidisciplinary Optimization*, 46(3):369–384, 2012. ISSN 1615-147X.

Bruyneel, M. SFP-a new parameterization based on shape functions for optimal material selection: application to conventional composite plies. *Structural and Multidisciplinary Optimization*, 43(1):17–27, JAN 2011. ISSN 1615-147X.

Bruyneel, M., Beghin, C., Craveur, G., Grihon, S., and Sosonkina, M. Stacking sequence optimization for constant stiffness laminates based on a continuous opti-

mization approach. *Structural and Multidisciplinary Optimization*, 46(6):783–794, 2012. ISSN 1615-147X.

Bruyneel, M., Duysinx, P., Fleury, C., and Gao, T. Extensions of the Shape Functions with Penalization Parameterization for Composite-Ply Optimization. *AIAA Journal*, 49(10):2325–2329, OCT 2011. ISSN 0001-1452.

Costin, D. P. and Wang, B. P. Optimum design of a composite structure with manufacturing constraints. *Thin-Walled Structures*, 17(3):185–202, 1993.

Courant, R. and Hilbert, D. *Methods of mathematical physics*, volume 1. Interscience Publishers, New York, 1953.

Duysinx, P. and Sigmund, O. New development in handling stress constraints in optimal material distribution. In *7th Symposium on Multidisciplinary Analysis and Optimization.*, pages 1501–1509, 1998. AIAA-98-4906.

Gao, T., Zhang, W., and Duysinx, P. A bi-value coding parameterization scheme for the discrete optimal orientation design of the composite laminate. *International Journal for Numerical Methods in Engineering*, 91(1): 98–114, 2012. ISSN 1097-0207.

Ghiasi, H., Pasini, D., and Lessard, L. Optimum stacking sequence design of composite materials Part I: Constant stiffness design. *Composite Structures*, 90(1):1–11, 9 2009.

Ghiasi, H., Fayazbakhsh, K., Pasini, D., and Lessard, L. Optimum stacking sequence design of composite materials Part II: Variable stiffness design. *Composite Structures*, 93(1):1–13, 12 2010.

Gill, P., Murray, W., and Saunders, M. SNOPT: An SQP algorithm for large-scale constrained optimization. *SIAM Review*, 47(1):99–131, 2005.

Groenwold, A. and Haftka, R. Optimization with non-homogeneous failure criteria like tsai-wu for composite laminates. *Structural and Multidisciplinary Optimization*, 32(3):183–190, 2006. ISSN 1615-147X.

Hvejsel, C. and Lund, E. Material interpolation schemes for unified topology and multi-material optimization. *Structural and Multidisciplinary Optimization*, 43(6): 811–825, 2011.

Hvejsel, C., Lund, E., and Stolpe, M. Optimization strategies for discrete multi-material stiffness optimization. *Structural and Multidisciplinary Optimization*, 44(2): 149–163, 2011.

Kassapoglou, C. *Design and Analysis of Composite Structures: With Applications to Aerospace Structures*, volume 1. John Wiley & Sons, New York, 2010. ISBN 978-0-470-97271-7.

Kennedy, G. J. and Martins, J. R. R. A. A laminate parametrization technique for discrete ply-angle problems with manufacturing constraints. *Structural and Multidisciplinary Optimization*, 2013.

Kim, C., Song, S., Hwang, W., Park, H., and Han, K. On the failure indices of quadratic failure criteria for optimal stacking sequence design of laminated plate. *Applied Composite Materials*, 1(1):81–85, 1994. ISSN 0929-189X.

Le, C., Norato, J., Bruns, T., Ha, C., and Tortorelli, D. Stress-based topology optimization for continua. *Structural and Multidisciplinary Optimization*, 41(4):605–620, 2010. ISSN 1615-147X.

Le Riche, R. and Haftka, R. T. Optimization of laminate stacking sequence for buckling load maximization by genetic algorithm. *AIAA*, 31(5):951–956, May, 1993.

Lindgaard, E. and Dahl, J. On compliance and buckling objective functions in topology optimization of snap-through problems. *Structural and Multidisciplinary Optimization*, 47(3):409–421, 2012.

Lindgaard, E. and Lund, E. Nonlinear buckling optimization of composite structures. *Computer Methods in Applied Mechanics and Engineering*, 199(37-40):2319–2330, 2010. ISSN 0045-7825.

Liu, B., Haftka, R. T., Akgün, M. A., and Todoroki, A. Permutation genetic algorithm for stacking sequence design of composite laminates. *Computer Methods in Applied Mechanics and Engineering*, 186:357–372, March 1999.

Liu, D., Toropov, V. V., Querin, O. M., and Barton, D. C. Bilevel Optimization of Blended Composite Wing Panels. *Journal Of Aircraft*, 48(1):107–118, JAN-FEB 2011. ISSN 0021-8669.

Lund, E. *Finite element based design sensitivity analysis and optimization*. Ph.D. Thesis, Institute of Mechanical Engineering, Aalborg University, Denmark, 1994. Special report no. 23.

Lund, E. Buckling topology optimization of laminated multi-material composite shell structures. *Composite Structures*, 91(2):158–167, NOV 2009. ISSN 0263-8223.

Lund, E. and Stegmann, J. On structural optimization of composite shell structures using a discrete constitutive parametrization. *Wind Energy*, 8(1):109–124, 2005.

Lund, E., Sørensen, R., and Sørensen, S. N. Multi-criteria multi-material topology optimization of laminated composite structures including local constraints. In *Book of Abstracts*, Orlando, Florida, 2013. 10th World Congress on Structural and Multidisciplinary Optimization.

Manne, P. M. and Tsai, S. W. Design Optimization of Composite Plates: Part II–Structural Optimization by Plydrop Tapering. *Journal of Composite Materials*, 32 (6):572–598, March 01 1998.

MUST. The MUltidisciplinary Synthesis Tool, 2013. http://www.must.m-tech.aau.dk.

Nemhauser, G. L. and Wolsey, L. A. *Integer and Combinatorial Optimization*. John Wiley & Sons, Inc, 1988. ISBN 0-471-82819-X.

Neves, M., Rodrigues, H., and Guedes, J. Generalized topology design of structures with a buckling load criterion. *Structural Optimization*, 10:71–78, 1995.

Niu, B., Olhoff, N., Lund, E., and Cheng, G. Discrete material optimization of vibrating laminated composite plates for minimum sound radiation. *International Journal of Solids and Structures*, 47(16):2097–2114, AUG 1 2010. ISSN 0020-7683.

Olhoff, N., Bendsøe, M. P., and Rasmussen, J. On cad-integrated structural topology and design optimization. *Computer Methods in Applied Mechanics and Engineering*, 89(1):259–279, 1991.

Overgaard, L., Lund, E., and Thomsen, O. Structural collapse of a wind turbine blade. Part A: Static test and equivalent single layered models. *Composites Part A: Applied Science and Manufacturing*, 41(2):257 – 270, 2010. ISSN 1359-835X.

Panda, S. and Natarajan, R. Analysis of laminated composite shell structures by finite element method. *Computers & Structures*, 14(3-4):225–230, 1981.

París, J., Navarrina, F., Colominas, I., and Casteleiro, M. Block aggregation of stress constraints in topology optimization of structures. *Advances in Engineering Software*, 41:433–441, 2010.

Rietz, A. Sufficiency of a finite exponent in simp (power law) methods. *Structural and Multidisciplinary Optimization*, 21(2):159–163, 2001.

Rodrigues, H., Guedes, J., and Bendsøe, M. Necessary conditions for optimal design of structures with a nonsmooth eigenvalue based criterion. *Structural Optimization*, 9:52–56, 1995.

Seresta, O., Gürdal, Z., Adams, D. B., and Watson, L. T. Optimal design of composite wing structures with blended laminates. *Composites Part B: Engineering*, 38(4):469–480, 6 2007.

Seyranian, A., Lund, E., and Olhoff, N. Multiple eigenvalues in structural optimization problems. *Structural Optimization*, 8:207–227, 1994.

Sørensen, S. N. and Lund, E. Topology and thickness optimization of laminated composites including manufacturing constraints. *Structural and Multidiciplinary Optimization*, 48:249–265, 2013.

Stegmann, J. and Lund, E. Discrete material optimization of general composite shell structures. *International Journal for Numerical Methods in Engineering*, 62(14):2009–2027, 2005.

Stolpe, M. and Svanberg, K. An alternative interpolation scheme for minimum compliance topology optimization. *Structural and Multidisciplinary Optimization*, 22 (2):116–124, 2001.

Svanberg, K. The method of moving asymptotes - a new method for structural optimization. *International Journal for Numerical Methods in Engineering*, 24(2):359–373, February 1987.

Svanberg, K. Some modelling aspects for the fortran implementation of MMA. *Technical report*, 2004.

Toropov, V. V., Jones, R., Willment, T., and Funnell, M. Weight and Manufacturability Optimization of Composite Aircraft Components Based on a Genetic Algorithm. In *Proceedings of 6th World Congress of Structural and Multidisciplinary Optimization (WCSMO)*. Rio de Janeiro, Brazil, May–June 2005.

Tsai, S. W. and Wu, E. M. A general theory of strength for anisotropic materials. *Journal of Composite Materials*, 5(1):58–80, 1971.

Wittrick, W. Rates of change of eigenvalues, with reference to buckling and vibration problems. *Journal of the Royal Aeronautical Society*, 66:590–591, 1962.

Zein, S., Colson, B., and Grihon, S. A primal-dual backtracking optimization method for blended composite structures. *Structural and Multidisciplinary Optimization*, 45(5):669–680, MAY 2012. ISSN 1615-147X.

Zhou, M. and Fleury, R. Composite Optimization - Ply Drop-Rate Constraints for Concepts and Detailed Design. In *Proceedings of the 23rd International Congress of Theoretical and Applied Mechanics (ICTAM)*. Beijing, China, August 2012.

Zhou, M., Fleury, R., and Kemp, M. Optimization of Composits - Recent Advances and Application. The 7th Altair CAE Technology Conference, Altair, 2011.